water

MDPI

Article

Hydrogeochemical Processes and Natural Background Levels of Chromium in an Ultramafic Environment. The Case Study of Vermio Mountain, Western Macedonia, Greece

Eleni Vasileiou [1], Panagiotis Papazotos [1], Dimitrios Dimitrakopoulos [2] and Maria Perraki [1,*]

[1] School of Mining and Metallurgical Engineering, Division of Geo-Sciences, National Technical University of Athens, 9 Heroon Polytechniou St., 15773 Zografou, Greece; elvas@metal.ntua.gr (E.V.); papazotos@metal.ntua.gr (P.P.)
[2] Researcher, Orologa 8, 11521 Athens, Greece; ddimitrakopoulos@gmail.com
* Correspondence: maria@metal.ntua.gr; Tel.: +30-2107722115

Abstract: The hydrogeochemical processes and natural background levels (NBLs) of chromium in the ultramafic environment of Vermio Mountain, Western Macedonia, Greece, were studied. Seventy groundwater samples were collected from 15 natural springs between 2014–2020, and an extensive set of physical and chemical parameters were determined. The ultramafic-dominated environment of western Vermio Mt. favors elevated groundwater concentrations of dissolved magnesium (Mg^{2+}), silicon (Si), nickel (Ni), and Cr in natural spring waters. Chromium was the principal environmental parameter that exhibited a wide range of concentrations, from 0.5 to 131.5 μg/L, systematically exceeding the permissible limit of 50 μg/L for drinking water. Statistical evaluation of hydrogeological, hydrochemical, and hydrological data highlighted the water-ultramafic rock process as the predominant contributor of Cr in groundwater. The NBL assessment for Cr and Cr(VI) was successfully applied to the typical ultramafic-dominated spring "Potistis" that satisfied all the methodology criteria. The NBLs of Cr and Cr(VI) were defined at 130 μg/L and 100 μg/L, respectively, revealing that a natural ultramafic-dominated environment exhibits the geochemical potential to contribute very high concentrations of geogenic Cr to groundwater. The holistic methodology, proposed herein, could be implemented in any catchment scale to assess geogenic and anthropogenic Cr-sources that degrade groundwater quality.

Keywords: chromium; ultramafic rocks; springs; water–rock interaction; natural background levels

Citation: Vasileiou, E.; Papazotos, P.; Dimitrakopoulos, D.; Perraki, M. Hydrogeochemical Processes and Natural Background Levels of Chromium in an Ultramafic Environment. The Case Study of Vermio Mountain, Western Macedonia, Greece. *Water* **2021**, *13*, 2809. https://doi.org/10.3390/w13202809

Academic Editors: Evangelos Tziritis and Andreas Panagopoulos

Received: 2 August 2021
Accepted: 2 October 2021
Published: 9 October 2021

1. Introduction

Natural background levels (NBLs) are defined as "the concentration of a substance or the value of an indicator in a body of groundwater corresponding to no, or only very minor, anthropogenic alterations to undisturbed conditions" according to the Groundwater Daughter Directive (GDD) (Directive 2006/118/EC) [1]. Broadly, the term of NBLs is synonymous with the terms of environmental geochemistry "natural/geochemical background values" or "geochemical baseline" used in the past [2]. The NBLs are a set of several varying hydrogeological (i.e., the residence time of groundwater in the saturated zone, recharge by precipitation, hydraulic connection with other aquifer systems) [3–5], and hydrogeochemical (i.e., water–rock interaction, pH/redox conditions, chemical, and biological processes in the unsaturated zone) [5–7] factors. The determination of NBLs requires in-depth knowledge of geological/hydrogeochemical processes [8] and the distinguishment of natural and anthropogenic factors that affect the groundwater systems [9]. The need to separate NBLs from the anthropogenic impacts (e.g., urbanization, industrialization, agricultural activity) is frequently satisfied through statistical and pre-selection (PS) methods [10]. Such methods were applied within the EU-Specific Targeted Research Project BRIDGE (Background cRiteria for the iDentification of Groundwater thrEsholds),

the objective of which was to develop a comprehensive methodology to evaluate threshold values (TVs) and NBLs of various qualitative parameters in the groundwater resources [11]. The first stage of this approach includes the PS method, which assumes that the groundwater samples represent pristine groundwater not affected by anthropogenic pressures [9]. It constitutes the most frequent method to exclude samples influenced by anthropogenic activities based on specific criteria such as concentrations of Cl^-, Na^+, NO_3^-, NH_4^+, and DO [6,10,12]. The PS method has been successfully applied to establish NBLs for different physical and chemical parameters, including EC, Cl^-, SO_4^{2-}, F^-, As, Cr, Cr(VI), Mn, Ni, Fe, and V in many European water bodies [4,5,7,13–17]. The next stage contains statistical tools such as box plots and normality tests for assessing the NBLs of the target chemical parameter. An approach that incorporates both PS and statistical methods has been performed by many researchers [7–10,14,15], providing a comprehensive methodology to boost the validity of the assessment, mainly when the geochemical and geological features are adequately considered [16]. Thus, the challenging assessment of NBLs in an environment in which the prevailing geochemical conditions favor the occurrence and mobilization of naturally occurring chemical elements could provide essential information regarding the controversial geogenic and anthropogenic inputs in a complex environmental setting.

The water–ultramafic rock interaction is of great scientific interest due to the high content of the latter in Cr (1000–3000 mg/kg), and other potentially toxic elements (PTEs) such as As, Co, Fe, Mn, and Ni compared to the Earth's crust composition [8–21] and to other rock types [22]; it constitutes the principal geogenic source of Cr in the environment [18]. Chromium is mainly hosted in spinels (e.g., chromite and magnetite) and silicates (e.g., pyroxene, serpentine, chlorite, olivine, talc). Serpentine group minerals can be highly enriched in Cr because it substitutes for magnesium (Mg) and/or iron (Fe) [18]. In the crystal lattice of most minerals, Cr occurs in the trivalent valence state [Cr(III)]. However, the geochemically immobile Cr(III) is oxidized into the mobile and toxic for the living organisms hexavalent chromium [Cr(VI)] in the presence of natural manganese oxides (MnO_2), specifically pyrolusite (b-MnO_2), in the typical range of groundwater pH (6.5–8.5) and under oxidizing redox potential (Eh) conditions [23–28]. Although an increasing number of studies focus on the occurrence and fate of Cr in the environment [29–38] only a few have systematically examined the geochemical fingerprint of water–ultramafic rock interaction in natural springs [29,33,35,39]. Typical worldwide examples of ultramafic springs with elevated groundwater concentrations of Cr(VI) have been recorded in the Province of La Spezia, Italy (up to 73 μg/L) [29], the Pollino massif, Italy (up to 30 μg/L) [40], the Gerania springs, Greece (up to 17.2 μg/L) [33], the Euboea Island, Greece (up to 37 μg/L) [41], and the Lesvos and Rhodes Islands, Greece (10–15 μg/L) [42]. The water–rock interaction constitutes a crucial and controlling factor concerning groundwater evolution. The geochemical reactions between the recharging water and the minerals of the host rocks affect the groundwater quality [43,44]. Hydrogeological and hydrogeochemical conditions such as pH, Eh, dissolved oxygen (DO), and groundwater flow path play a significant role in elevated concentrations of PTEs, including Cr, in the aquifer systems. Geochemical reactions such as ion exchange, weathering, precipitation/dissolution, and sorption process control the groundwater's composition considerably. During chemical weathering, some major ions, PTEs, and other trace elements become mobile and release from the parent rocks to the groundwater along the flow path. In addition, the mobility and solubility of these elements are controlled by water–rock contact time, Eh–pH conditions, and chemical reactions with organic matter [36]. Ionic ratios, saturation indices (SIs), and geochemical bivariate plots are usually evaluated to determine the intensity of water–rock interaction and chemical reactions [43]. Hence, the primary target of studying the mechanism of water–rock interaction is to elucidate the indissoluble association between the geological environment and the qualitative characteristics of groundwater.

In this work, we study the geochemical fingerprint of the water–ultramafic rock interaction process in the western Vermio Mt., Western Macedonia, Greece, and determine the NBLs of Cr in groundwater from natural springs. At the catchment scale of the

Sarigkiol Basin, elevated groundwater concentrations of Cr (up to ~140 μg/L) have been recorded in irrigation wells in the lowland [45]. Based on geospatial and multivariate statistical analyses of data from selected natural springs, irrigation wells, and surface waters the increased concentrations of Cr were attributed mainly to geogenic origin with the synergistic contribution of anthropogenic factors [45]. Challenged by the leaching potential of Cr of the ultramafic rocks in the area, we focus, herein, exclusively on the natural springs located in the ultramafic environment of western Vermio Mt, assessing hydrogeochemical data of a 7-year monitoring period (2014–2020). The springs are ideal for setting the NBLs at the catchment scale of the Sarigkiol Basin, because: (a) they record a strong ultramafic footprint, (b) they are located at a high altitude (>1300 m), (c) they exhibit unique worldwide high to very high concentrations of Cr (up to ~130 μg/L) [45], and (d) they are not affected by anthropogenic activities. Defining the NBLs of Cr in western Vermio Mt., will facilitate the identification of Cr origin in groundwater in the Sarigkiol Basin. This is the first systematic study of the natural springs of western Vermio Mt. and provides important hydrogeochemical data for the geogenic footprint of a natural ultramafic environment on the groundwater quality.

2. Materials and Methods

This section contains basic information about the: (i) study area, (ii) geological and hydrogeological setting, and (iii) sampling, chemical analysis procedures, and data processing.

2.1. Case Study

The present study is focused on the western Vermio Mt., located in the eastern part of the Sarigkiol Basin, Western Macedonia, Greece. The altitude of Vermio Mt is 2025 m and the average altitude of the basin is 650 m. The study area lies between the latitudes 40°25′00″ and 40°28′00″ E and the longitudes 21°56′00″ and 22°59′00″ N (Figure 1). In this area, any extensive anthropogenic activities lack except for local livestock farming and sporadically logging.

2.2. Geological and Hydrogeological Setting

The western Vermio Mt. is composed of (Figures 1 and 2) [46,47]: (a) alluvial deposits, (b) clastic conglomerates, talus cones, and breccias, (c) upper Cretaceous flysch, (d) a complex of schists and cherts formations, (e) ultramafic rocks (serpentinites and peridotites), (f) Triassic–Jurassic limestones, (g) Cretaceous limestones.

The aquifer systems in Vermio Mt. are:

(a) The deep karstic aquifer of the Triassic-Jurassic limestones, which form the mountainous boundaries and the basement of the Sarigkiol Basin,
(b) Perched aquifer systems that are developed in the highly fractured serpentinites of Vermio Mt. due to secondary porosity,
(c) Small in size and capacity, karstic aquifers developed in the scattered Cretaceous limestones. There are many aquifers in which the water table varies from +700 up to +900 m. They are hydraulically connected and recharge the groundwater of the screes and talus cones in the ridges of the basin. The general flow direction of the groundwater is from the mountainous area to the center of the basin, i.e., NE–SW.

Different types of natural springs flow out in Vermio Mt. and specifically (Figure 1):

Contact springs formed where permeable formations (limestones, breccia, conglomerates) overlay formations of low permeability or impermeable (altered ultramafic rocks/serpentinites). Contact springs studied here were: the springs S19, S10, S15 in the Agio Pnevma area, the "Potistis"-W13 spring, the spring S1 in the Agios Dimitrios area, the spring "Mouratidis"-S2, the springs S13, S14 in the Agios Panteleimonas area, and the springs S5 and S6 in the Vazelona area.

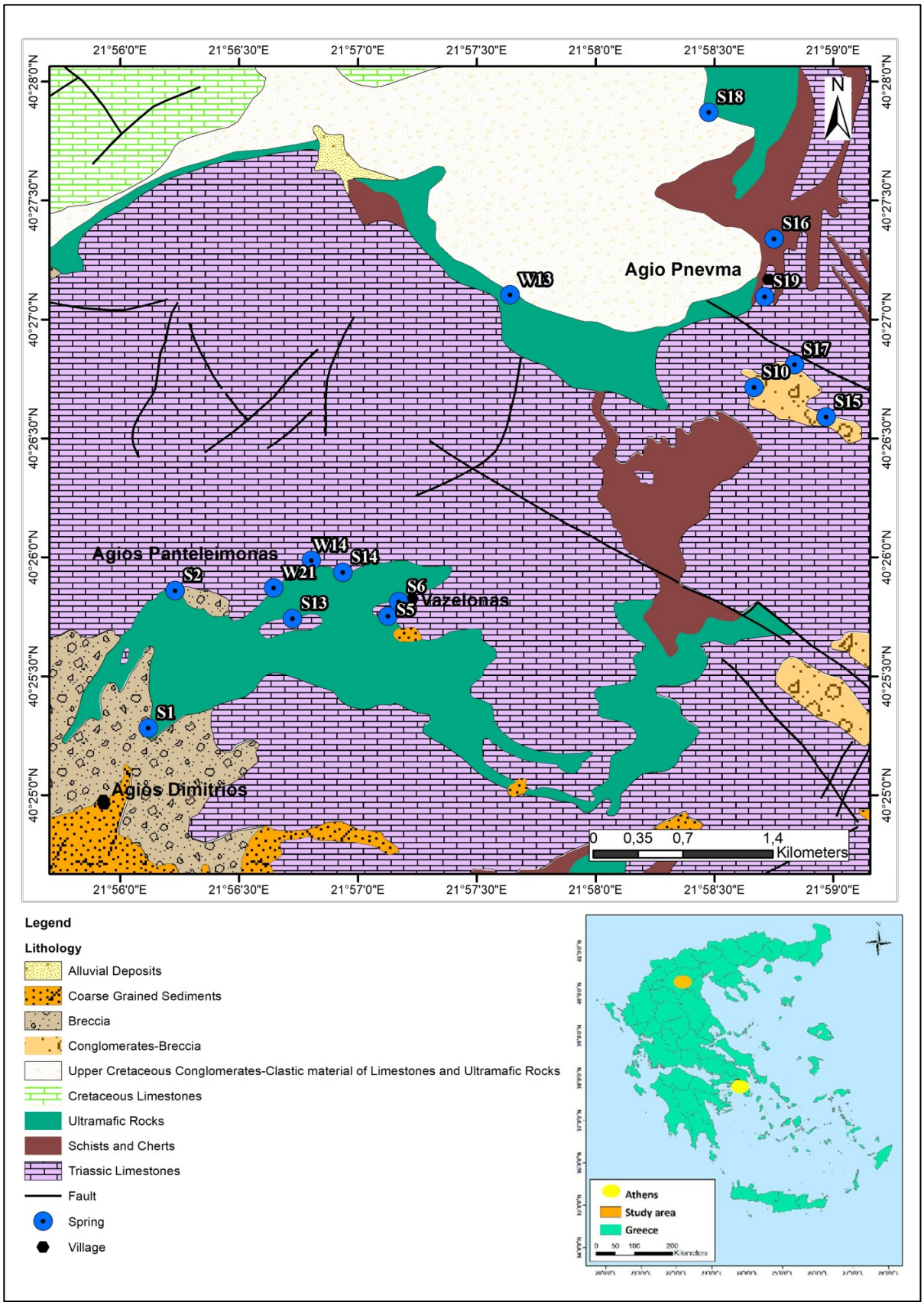

Figure 1. A simplified geological map of the western Vermio Mt.; the natural springs studied herein are marked.

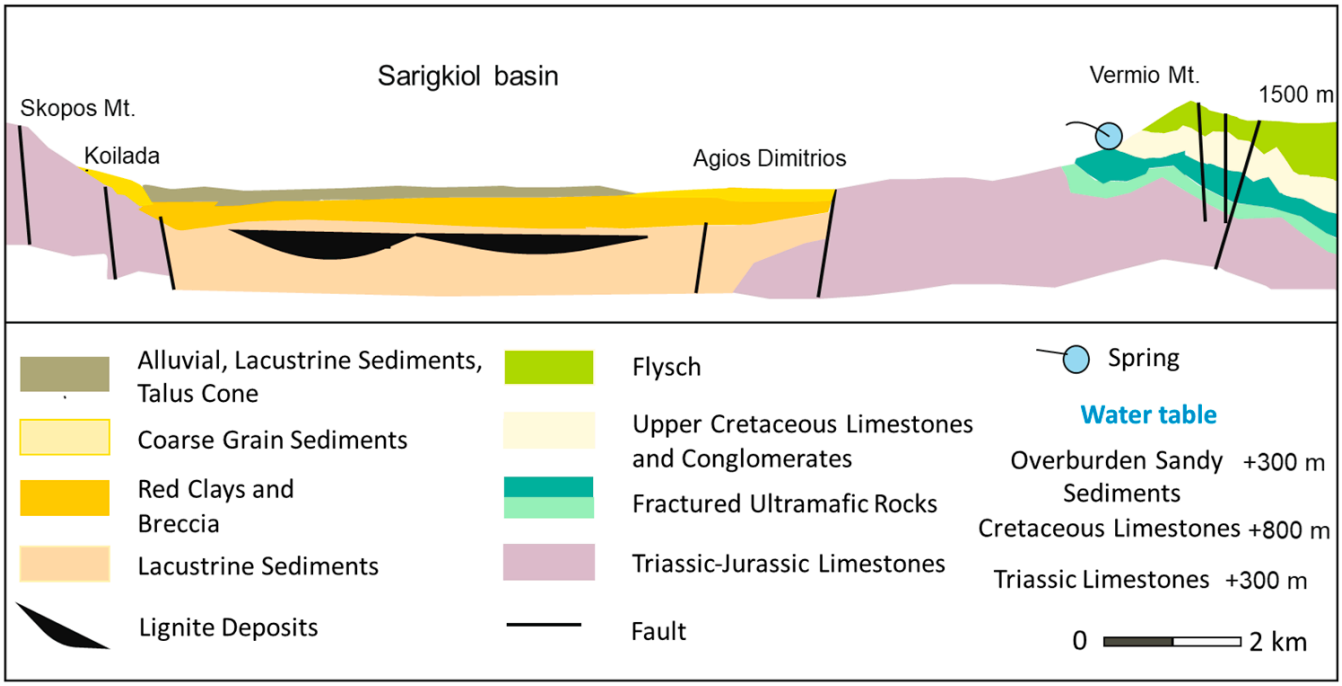

Figure 2. A simplified geological section of the western Vermio Mt.

Fault springs formed where impermeable rocks such as ultramafic rocks are in contact with an unconfined aquifer due to faulting; the springs "Elafakia"-W14 and W21 in the Agios Panteleimonas area belong to this type.

The spring "Potistis"-W13, presents great interest, because of the very high concentrations of Cr it exhibits [45]. The spring "Potistis"-W13 flows out at an elevation of 1300 m in an ultramafic environment characterized by the absence of any anthropogenic activities. It constitutes a contact-type spring in the contact of conglomerates with ultramafic clastic material and limestones and ultramafic rocks. The aquifer, which discharges via the spring, flows through a weathered zone in serpentines. The natural recharge comes mainly from the seasonal precipitations via the permeable upper unsaturated zone (conglomerates, clastic material of ultramafic rocks, and limestones). The recharge water is mainly enriched with released PTEs (mainly Cr) from the ultramafic rocks, as the rainfall infiltrates through the weathered fractured ultramafic rocks. An additional lateral recharge takes place due to secondary porosity in the fractured ultramafic rocks. The high permeability of the unsaturated zone due to the presence of conglomerates in this area facilitates the direct recharge of the aquifer in a short time. The range of discharge was calculated from 205 L/h up to 1200 L/h, with an average value of 482 L/h. In Figure 3, the simplified hydrogeological section describes the natural recharge and the operation mechanism of the spring "Potistis"-W13.

In western Vermio Mt. ultramafic rocks, mainly serpentinites, carbonates, schists and cherts occur [48]. The main mineral phases of the ultramafic rocks, depending on the degree of serpentinization, are serpentine [$(Mg, Mn, Fe, Co, Ni)_{3-x}SiO_2O_5(OH)_4$], olivine [$(Mg,Fe^{2+})_2(SiO_4)$]), pyroxene [$(Mg,Fe^{2+})(Si,Al)_2O_6$], talc [$Mg_3Si_4O_{10}(OH)_2$], chlorite [$(Mg,Fe^{2+})_5Al(Si_3Al)O_{10}(OH)_8$], tremolite [$Ca_2(Mg,Fe^{2+})_5Si_8(OH)_2O_{22}(OH)_2$], magnetite ($Fe^{2+}Fe_2^{3+}O_4$) and Cr-rich magnetite [$Fe^{2+}(Fe^{3+},Cr)_2O_4$] and chromite ($FeCr_2O_4$).

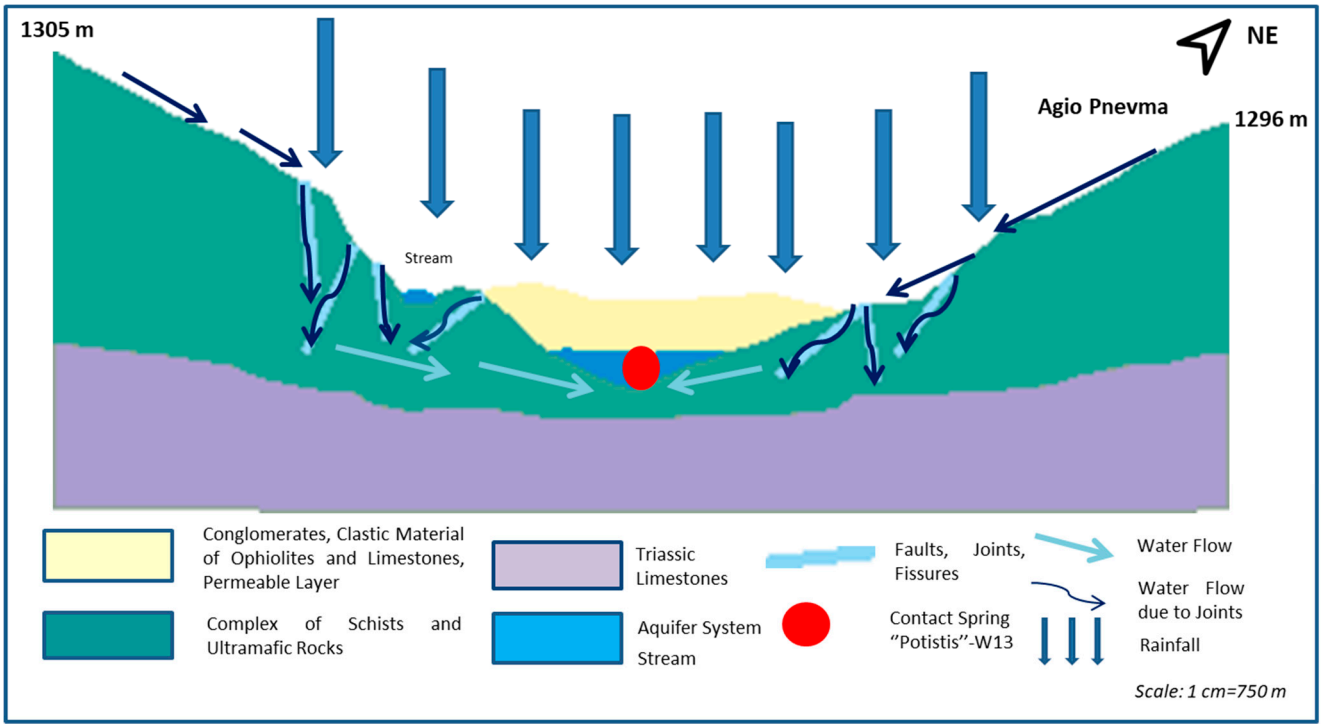

Figure 3. Simplified hydrogeological section of the natural spring "Potistis"-W13 in western Vermio Mt.

2.3. Sampling, Chemical Analyses, and Data Treatment

Springs to be systematically studied herein were selected based on their hydrogeochemical characteristics [45]. A total of 70 representative groundwater samples were collected from 15 natural springs during wet and dry periods from March 2014 to September 2020, following the groundwater sampling guidelines [49]. The 15 sampling sites (Figure 1) were classified into seven groups according to their location, lithology, and type: (i) twenty-three (23) samples were collected from the spring "Potistis"-W13, (ii) seven (7) samples from the Agio Pnevma area (S18, S16, S19, S10, S17, S15), (iii) twenty-three (23) samples from the spring "Elafakia"-W14, (iv) three (3) samples from the Agios Panteleimonas area (S13, S14, W21), (v) ten (10) samples from the spring "Mouratidis"-S2 (vi) two (2) samples (S5 and S6) from the Vazelona area, and (vii) two (2) samples from the spring S1 in the Agios Dimitrios area. Considering that the number of the water samples differs between the seven groups, each group has been treated and evaluated separately (the statistical and geochemical analysis), so the analyses are classified as reliable.

The analytical methods for the determination of physical [i.e., temperature (T), pH, oxidation-reduction potential (ORP), DO, and electrical conductivity (EC)] and chemical parameters (i.e., major ions, PTEs, and other trace elements) are provided in detail in Papazotos et al. [33]. The calculations of Eh and the total dissolved solids (TDS) values were carried out by converting ORP measurements (i.e., adding 200 mV) and the summation of major ions in each collected water sample, respectively.

AquaChem 5.0 software was used to elaborate chemical analyses, develop a Piper diagram, and calculate alkalinity. The statistical analyses of the chemical data were performed with SPSS 22.0 software.

2.4. Spearman's Rank Correlation Coefficient

Spearman's rank correlation coefficient (ρ, also signified by r_s) measures the strength and direction of association between two ranked variables, evaluating the degree of linear association or correlation between these independent variables. It presents many similarities to Pearson's coefficient except that it operates on the ranks of the data rather than the raw data [50].

The Spearman's rank correlation coefficient is calculated according to the following Equation (1) [51]:

$$r_s = \frac{6\sum_{i=1}^{n} d_i^2}{n(n^2-1)} \quad (1)$$

where d_i = difference in paired ranks, n = number of cases, x_i and y_i = data pair.

The formula to use when there are tied ranks is Equation (2):

$$\rho = \frac{\sum_i \left(x_i - \bar{x}\right)\left(y_i - \bar{y}\right)}{\sqrt{\sum_i \left(x_i - \bar{x}\right)^2 \sum_i \left(y_i - \bar{y}\right)^2}} \quad (2)$$

The Spearman's rank correlation coefficient, r_s, can get values from -1 to +1. The equation for the calculation is developed so that it gives r_s = +1 when the data pairs have a perfect positive correlation ($d^i = 0$) and $r_s = -1$ for the perfect negative correlation, whereas $r_s = 0$ indicates no association between ranks. The closer r_s is to zero the weaker the association between the ranks is.

The values of the correlation coefficient are classified as very strong (0.80–1), strong (0.60–0.79), moderate (0.40–0.59), weak (0.20–0.39), and very weak (0.00–0.19) [52]. The correlation coefficient is highly statistically significant, marginally statistically significant when the *p*-value is $p < 0.01$, $p < 0.05$.

2.5. Shapiro-Wilks Test

Shapiro–Wilks is a test of normality in frequentist statistics. The null hypothesis of this test is that the dataset is normally distributed. Thus, if the *p*-value is less than the chosen alpha level (0.05 in this case), then the null hypothesis is rejected and the data tested are not normally distributed. If the *p*-value is greater than the selected alpha level, then the null hypothesis cannot be rejected (Equation (3)) [53].

$$W = \frac{\sum_{i=1}^{n} \left(a_i x_{(i)}\right)^2}{\sum_{i=1}^{n} \left(x_i - \bar{x}\right)^2} \quad (3)$$

where $x_{(i)}$ is the i-th largest order statistic, x- is the sample mean, and n is the number of observations.

2.6. Quantile–Quantile Plot

The quantile-quantile (q–q) plot is a graphical tool for defining if two datasets come from populations with a common distribution [54], basically tests the conformity between the empirical distribution and the given theoretical one. On a Q–Q plot normally distributed data, the points in a Q–Q plot will fit on a straight diagonal line.

2.7. Geochemical modeling

The geochemical software PHREEQC version 3.1.2 [55] coupling with the MINTEQ database was used to calculate the saturation indices (SIs) of natural spring samples. Mineral SIs employed to define mineral dissolution and precipitation processes in the natural springs of western Vermio Mt. Saturation index is calculated by the Equation (4):

$$SI = \mathrm{Log}\frac{IAP}{K_{sp}} = \mathrm{Log}IAP - \mathrm{Log}K_{sp} \quad (4)$$

where IAP = ion activity and K_{sp} = solubility product constant.

A positive SI indicates that the mineral is oversaturated or supersaturated with respect to the solution [56]; thus, the mineral could precipitate. Conversely, a negative SI indicates

that the solution is undersaturated with respect to the selected mineral, suggesting that the mineral is dissolved in groundwater to reach equilibrium.

2.8. Calculation of NBLs of Cr

The assessment of NBLs for the target parameter was implemented based on the BRIDGE methodology [11]. The applied modified multi-method was separated into three steps: (a) the hydrogeochemical (bivariate plots, Piper, SI), (b) the PS method, and (c) the statistical analysis for estimating the NBLs (box plots for outliers, Q–Q (quantile–quantile) plots, and normality tests).

The applied methodology for the assessment of NBLs of Cr is described in detail in Figure 4. The pre-selection (PS) method, which is widely applied worldwide, was employed to select the suitable spring water samples for the NBLs assessment [10,16,57–60]. The PS method constitutes the methodology geochemical approach to validate the dataset according to similar geochemical characteristics and recognize the water samples that are affected by anthropogenic activities. In the first stage, the hydrochemical facies were selected based on the DO concentrations and Eh (ORP) [61]. The first dataset group included the water samples with ORP > 100 mV and DO > 3 mg/L. All water samples from the natural springs satisfied this criterion. The next criterion included consideration of redox conditions; if the prevailing conditions were oxidizing, then the concentrations of NO_3^- < 10 mg/L would be considered and if the conditions were reducing, then the NH_4^+ < 0.5 mg/L would be considered [9,61,62] to exclude the samples affected by anthropogenic activities [62,63]. Based on this criterion, the samples with NO_3^- > 10 mg/L were considered to be affected by anthropogenic activities and thus, were excluded from the new dataset. The next criterion required eight measurements per year for two years or two measurements per year for at least four years to exist for each spring [16].

2.9. Threshold Values (TVs) Derivation

The assessment of TVs was based on three scenarios [11,58] (Figure 5). The reference value was set equal to the water drinking acceptable limit (i.e., World Health Organization (WHO) guideline value).

2.10. Meteoric Genesis Index (MGI)

The meteoric genesis index (MGI) was also employed to classify the groundwater sources based on the depth of the meteoric water [64]. This index was calculated using the following Equation (5):

$$r_2 = Na^+ + K^+ - \frac{Cl^-}{SO_4^{2-}}, \text{ all concentrations are expressed in meq/L} \quad (5)$$

when r_2 < 1, the groundwater source is of deep meteoric water percolation type whereas when r_2 > 1 the groundwater is of shallow meteoric water percolation type [65].

2.11. Meteorological Data

Daily and monthly rainfall data for the period 2014–2019 were evaluated from the meteorological station in the Ermakia village (40°30′325″ N, 21°51′233″ E) which is the most representative and the nearest one, located on Vermio Mt., at an elevation of 1100 m. The annual precipitation for the period 2014–2019 was estimated at 985 mm.

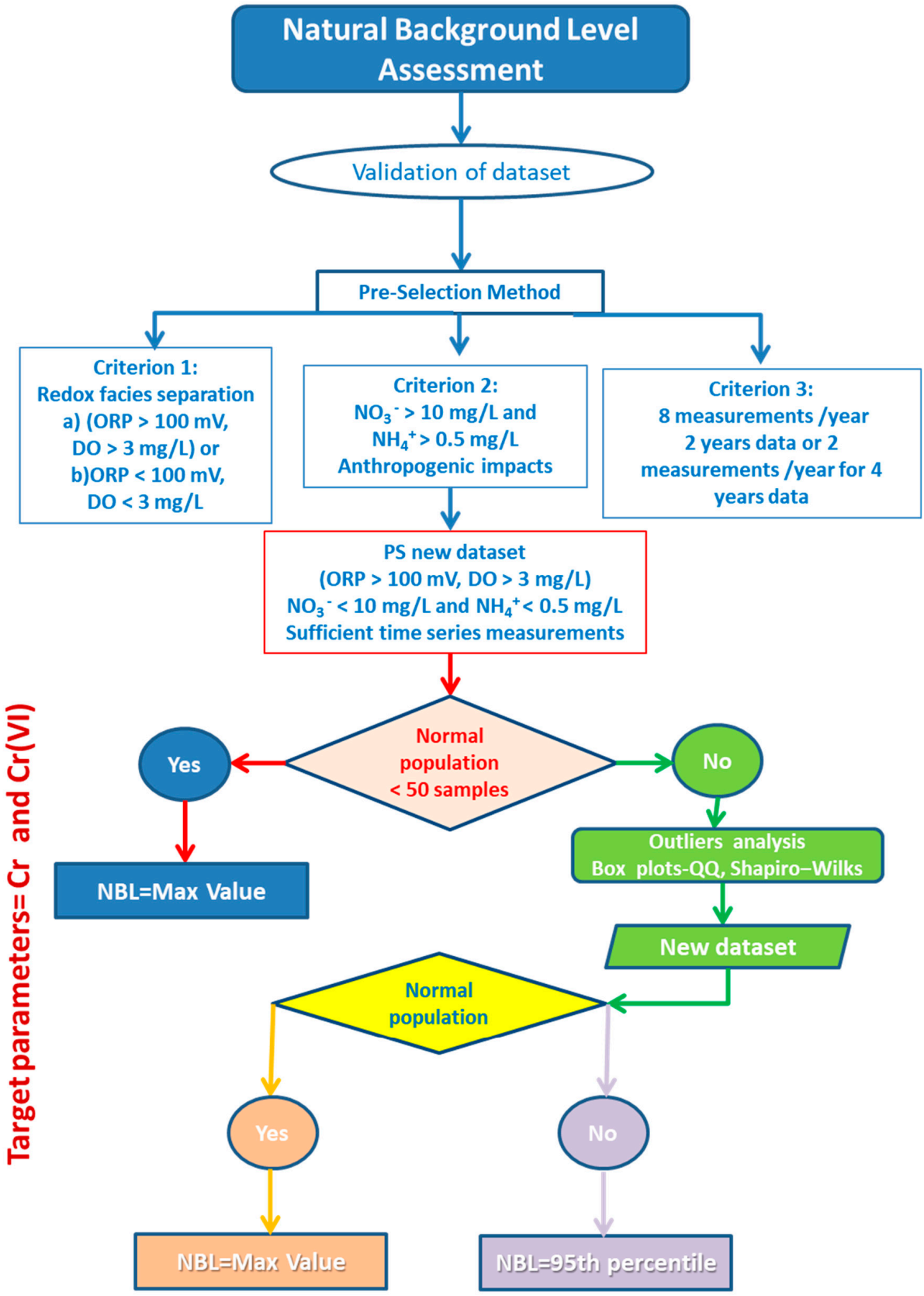

Figure 4. Flow chart of the modified conceptual model for the assessment NBLs of the target parameter.

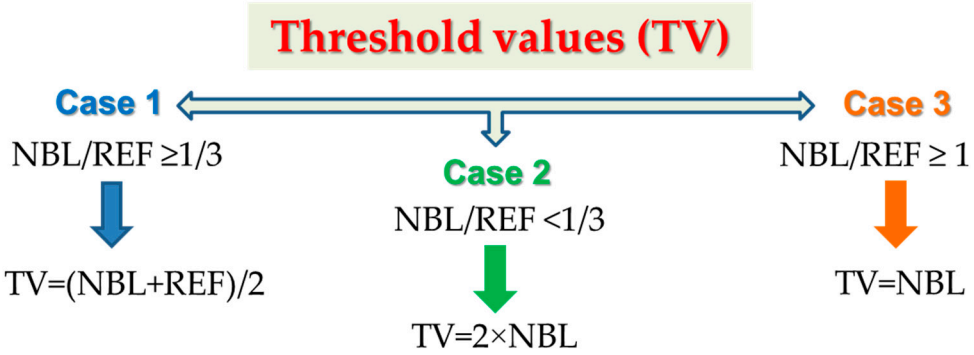

Figure 5. Flow chart for the assessment TVs for the target parameter.

3. Results

3.1. Chemometric Analysis

All chemical analyses were grouped into the above-mentioned seven categories according to their location, lithology, and type to evaluate the results. The descriptive statistics (max, min, median) of the physical and chemical parameters, for the studied spring waters from March 2014 until October 2020, are summarized in Tables 1 and 2. Some concentrations above the detection limit (DL) and below the quantification limit (QL) were not excluded because their very low concentrations do not affect the data processing of this work. All concentrations determined by ICP–MS presented a QL equal to the DL. The parameters NO_2^-, NH_4^+, PO_4^{3-}, Fe, Cd, Co were measured below the detection limit (BDL) in the majority of the samples. Silver, Au, Be, Bi, Cs, Pt, Re, Ga, Ge, Hf, Hg, In, Mo, Nb, Ta, Ti, Th, Tl, W, Zr were detected BDL in all water samples. Hence, these elements were excluded from the statistical analyses. In Table 3, the dataset for Cr-Cr(VI) and the geographical coordinates for the sampling points are given.

In the Agios Panteleimonas area, the natural spring "Elafakia"-W14 and in the Agio Pnevma area, the natural spring "Potistis"-W13 were examined separately from the other springs in these areas because of their elevated groundwater concentrations of Cr.

Box plots depicting the variation of eight groundwater quality parameters (pH, Eh, DO, EC, Ca^{2+}, Mg^{2+}, HCO_3^- and Si) are given in Figures 6 and 7. The alkalinity of the water samples was calculated in a range of 1.95×10^{-3} meq/L (S18) up to 6.71×10^{-3} meq/L "Potistis"-W13, with an average value of 4.60×10^{-3} meq/L.

The abundance of major ions varied significantly among the natural springs (Table 4). Concentrations of Cr and Cr(VI) exhibited a wide range of values (Tables 1–3, Figures 8–11). Most physical and chemical parameters (e.g., EC, NO_3^-, SO_4^{2-}, As, B, Ba, Cd, Cu, Ni, Pb, Sb, Se, Zn, etc.) in the natural springs of Vermio Mt. exhibited lower concentrations than the desirable and permissible limits for drinking water. All samples were compared with the guideline of WHO for drinking water [66]. Exceedances were recorded in the natural springs "Potistis"-W13, "Elafakia"-W14, S1-Agios Dimitrios area, and S18- Agio Pnevma area. Specifically, in the spring S18-Agio Pnevma area, concentrations of K^+ exceeded the guideline value of 12 mg/L for drinking water (WHO, [66]). Two exceedances of As, above the permissible limits of 10 μg/L, were recorded in the natural spring S1 of the Agios Dimitrios area. In the spring "Elafakia"-W14 seven water samples exceeded the WHO guideline value of 50 μg/L for Cr concentration for drinking water [66], while in the spring "Potistis"-W13 23 water samples exceeded this value. Finally, in total, three samples (one from the spring "Elafakia"-W14, and two from the spring "Potistis"-W13) exceeded the limit of 20 μg/L for the concentration of Ni for drinking water [66]. The systematic exceedances of Cr in the natural springs of Vermio Mt. were the principal reason for selecting Cr as the target parameter for NBLs assessment in this area.

Table 1. Maximum, minimum, and median values of physical and chemical parameters of natural springs in western Vermio Mt.

Parameter	Unit	QL	DL	The Agio Pnevma Area			The Agios Panteleimonas Area			"Mouratidis"			The Agios Dimitrios Area			The Vazelona Area		
				Max	Min	Median	Max	Min	Median	Max	Min	Median	Max	Min	Median	Max	Min	Median
pH	-	-	-	8.4	7.6	7.9	7.94	7.37	7.38	8.4	7.8	8.1	8.5	8.1	8.3	7.7	7.7	7.7
DO	mg/L	-	-	9.6	8.4	8.9	9.3	7.74	8.53	9.2	7.8	8.8	8.9	8.1	8.5	9.5	8.3	8.9
T	°C	-	-	16.0	10.8	14.3	18.0	13.1	13.6	25.6	9.8	13.8	24.1	8	16.1	15.8	15.0	15.4
TDS	mg/L	-	-	561.3	150.5	226.0	397.69	361.25	377.36	398	294.4	369.8	377	319.3	348.2	462.2	383.5	422.9
EC	µS/cm	10	-	593.0	293.0	460.0	505.0	448.0	494.0	520	405	426.8	456	446	451	484.0	389.0	436.5
Eh	mV	-	-	320.0	110.0	160.0	389.7	303.0	387.0	409	303.42	346.2	377	340.7	358.9	301.0	297.0	299.0
Ca^{2+}	mg/L	0.2	0.05	119.0	24.0	43.8	94.9	41.6	93.2	60.4	54.2	55.2	49.5	46.6	48.1	104.0	98.2	101.1
Mg^{2+}	mg/L	1.0	0.3	24.9	3.7	8.4	38.8	3.13	11.4	34.9	21.3	21.4	31.8	30.9	31.4	13.5	3.1	8.3
Na^{+}	mg/L	5.0	0.5	1.4	1.4	1.4	2.5	BDL	1.25	1.7	BDL	1.4	1.2	BDL	0.6	2.1	1.0	1.6
K^{+}	mg/L	0.2	0.05	33.0	0.4	0.6	1.63	0.59	1.22	1	0.3	0.3	1.8	1.5	1.7	10.8	1.4	6.1
NO_3^{-}	mg/L	5.0	1	BDL	BDL	BDL	BDL	BDL	BDL	9.1	8.3	8.7	BDL	BDL	BDL	1.0	BDL	BDL
Cl^{-}	mg/L	5.0	1	31.0	2.0	7.5	BDL	BDL	BDL	5	BDL	BDL	BDL	BDL	BDL	12.0	1.0	6.5
SO_4^{2-}	mg/L	10.0	2	31.0	10.0	20.5	19.0	12.0	19.0	20	16	16	22	BDL	11	21.0	13.0	17.0
HCO_3^{-}	mg/L	10.0	2	387.0	119.0	167.0	276.0	250.0	271.0	277	192	258	271	240	255.5	304.0	259.0	281.5
Al	µg/L	DL	1	8.0	2.0	3.0	1.0	1.0	1.0	1546	2	4	31	3	17	3.0	2.0	2.5
As	µg/L	DL	0.5	0.7	0.6	0.7	5.4	0.6	1.5	6.1	1.4	1.7	49.1	28.8	39	1.8	0.5	1.2
B	µg/L	DL	5	9.0	5.0	6.0	12.0	12.0	12.0	11	7	9	10	10	10	19.0	15.0	17.0
Ba	µg/L	DL	0.05	11.6	1.9	2.6	8.69	5.72	5.81	13.8	6	6.9	16.1	14.4	15.2	7.0	6.4	6.7
Br	µg/L	DL	5	25.0	8.0	13.0	14.0	11.0	12.0	16	13	14	15	9	12	15.0	13.0	14.0
Cr	µg/L	DL	0.1	47.8	0.5	3.8	18.0	1.5	1.9	38.3	10	20.4	16.6	10.9	13.8	0.8	0.5	0.7
Cr(VI)	µg/L	DL	0.1	36.7	0.5	1.8	7.2	1.0	1.0	33.9	7	16	16.5	8.7	12.6	0.5	0.1	0.3
Cu	µg/L	DL	0.1	2.8	0.9	1.2	1.2	0.6	0.7	2	0.7	1.4	1.3	1.1	1.2	2.8	1.1	2.0
Li	µg/L	DL	0.1	0.7	0.3	0.6	4.3	0.1	0.2	3.4	0.5	0.6	4.7	3.6	4.2	0.2	0.1	0.2
Mn	µg/L	DL	0.05	5.8	0.2	0.8	0.43	0.28	0.29	1.3	0.6	0.8	1.4	0.4	0.9	0.4	0.3	0.4
Ni	µg/L	DL	0.2	1.7	1.0	1.4	1.3	0.8	1.05	7.7	0.5	4.1	5.8	3.6	4.7	1.0	0.7	0.9
P	µg/L	DL	10	117	12.0	57.0	31.0	15.0	23.0	39	37	39	45	13	29	28.0	18.0	23.0
Si	µg/L	DL	40	14,327	2231	4296	24,875	3250	3441	21,350	8786	10,697	19,307	17,245	18,276	3495	3467	3481
Sr	µg/L	DL	0.01	84.0	44.5	59.8	79.03	41.76	70.15	62.9	57.5	58.4	65.2	60.7	62.9	83.2	69.7	76.5
U	µg/L	DL	0.02	0.2	BDL	0.1	7.2	0.4	0.7	0.3	0.3	0.3	0.4	0.3	0.3	0.7	0.2	0.4
V	µg/L	DL	0.2	0.7	0.2	0.3	0.08	0.08	0.08	4.6	1.3	1.5	4.7	4.3	4.5	0.8	0.5	0.7
Zn	µg/L	DL	0.5	12.7	7.5	10.4	4.3	3.4	3.9	14.8	9	13	11.9	7.3	9.6	33.1	13.6	23.4

BDL: Below the detection limit. DL: Detection limit. QL: Quantification limit.

Table 2. Maximum, minimum, and median values of physical and chemical parameters of the natural springs in western Vermio Mt.

Parameter	Unit	QL	DL	Potistis			Elafakia		
				Max	Min	Median	Max	Min	Median
pH	-	-	-	8.3	7.3	7.9	8.3	7.3	7.7
DO	mg/L	-	-	9.6	8.5	9.0	11.6	8.6	9.2
T	°C	-	-	15.2	6.2	12.3	20.5	5.8	12.5
TDS	mg/L	-	-	528.9	386.3	481.8	522.5	366.4	458.0
EC	µS/cm	10	-	620.0	374.8	574.5	718.0	357.7	546.0
Eh	mV	-	-	359.8	90.0	325.5	377.6	194.9	309.8
Ca^{2+}	mg/L	0.2	0.05	56.1	28.6	35.6	91.4	51.7	76.9
Mg^{2+}	mg/L	1.0	0.3	73.3	34.2	61.7	36.6	24.8	30.3
Na^{+}	mg/L	5.0	0.5	1.2	1.2	1.2	2.5	BDL	2.0
K^{+}	mg/L	0.2	0.05	0.5	0.1	0.3	3.1	0.6	0.7
$NO_3{}^{-}$	mg/L	5.0	1	BDL	BDL	BDL	1.0	BDL	BDL
Cl^{-}	mg/L	5.0	1	1.0	DL	1.0	8.0	BDL	2.0
$SO_4{}^{2-}$	mg/L	10.0	2	BDL	BDL	BDL	128.0	16.0	23.0
$HCO_3{}^{-}$	mg/L	10.0	2	409.0	298.0	382.0	369.0	250.0	318.0
Al	µg/L	DL	1	111.0	1.0	3.0	13.0	1.0	2.0
As	µg/L	DL	0.5	BDL	BDL	BDL	1.7	0.9	1.5
B	µg/L	DL	5	13.0	8.0	10.5	27.0	6.0	14.0
Ba	µg/L	DL	0.05	10.4	4.2	4.8	16.2	10.4	15.0
Br	µg/L	DL	5	18.0	10.0	14.0	28.0	18.0	21.0
Cr	µg/L	DL	0.1	131.5	39.0	103.9	57.4	26.0	47.5
Cr(VI)	µg/L	DL	0.1	100.0	39.0	90.0	51.2	18.0	41.0
Cu	µg/L	DL	0.1	4.0	0.3	0.5	6.4	0.6	1.3
Li	µg/L	DL	0.1	1.0	0.7	0.8	1.2	0.9	1.1
Mn	µg/L	DL	0.05	0.8	0.1	0.4	0.8	0.2	0.3
Ni	µg/L	DL	0.2	38.2	2.7	5.5	314.0	5.1	7.0
P	µg/L	DL	10	78.0	13.0	38.0	147.0	18.0	32.0
Si	µg/L	DL	40	22,394	15,120	20,663	17,717	13,248	14,685
Sr	µg/L	DL	0.01	40.3	32.0	35.2	90.4	58.3	74.0
U	µg/L	DL	0.02	0.1	BDL	BDL	1.1	0.6	0.8
V	µg/L	DL	0.2	1.6	0.2	0.4	1.2	0.7	1.0
Zn	µg/L	DL	0.5	37.3	4.1	5.1	74.7	4.6	8.7

BDL: Below the detection limit. DL: Detection limit. QL: Quantification limit.

Table 3. Geographical coordinates of the water sampling sites and the results of Cr-Cr(VI) for the natural springs in western Vermio Mt.

Sample ID	Latitude	Longitude	Sampling Point	Cr (μg/L)	Cr(VI) (μg/L)	Sample ID	Latitude	Longitude	Sampling Point	Cr (μg/L)	Cr(VI) (μg/L)
W13_06_2018	40°27′103″	21°57′639″	Potistis	41.6	39.2	W14_9a_2018	40°25′854″	21°56′878″	Elafakia	46.0	43.0
W13_07_2018	40°27′103″	21°57′639″	Potistis	39.0	39.0	W14_9b_2018	40°25′854″	21°56′878″	Elafakia	56.1	40.0
W13_09_2018a	40°27′103″	21°57′639″	Potistis	111.5	90.0	W14_9c_2018	40°25′854″	21°56′878″	Elafakia	56.3	40.0
W13_09_2018b	40°27′103″	21°57′639″	Potistis	109.5	90.0	W14_9d_2018	40°25′854″	21°56′878″	Elafakia	56.0	40.0
W13_09_2018c	40°27′103″	21°57′639″	Potistis	108.7	90.0	W14_9e_2018	40°25′854″	21°56′878″	Elafakia	54.5	41.0
W13_09_2018d	40°27′103″	21°57′639″	Potistis	112.6	90.0	W14_05_2019	40°25′854″	21°56′878″	Elafakia	42.5	40.0
W13_10_2018a	40°27′103″	21°57′639″	Potistis	131.5	100.0	W14_08_2019	40°25′854″	21°56′878″	Elafakia	44.8	33.0
W13_10_2018b	40°27′103″	21°57′639″	Potistis	130.2	100.0	W14_11_2019	40°25′854″	21°56′878″	Elafakia	46.3	41.0
W13_10_2018c	40°27′103″	21°57′639″	Potistis	111.9	90.0	W14_02_2020	40°25′854″	21°56′878″	Elafakia	47.5	32.0
W13_10_2018d	40°27′103″	21°57′639″	Potistis	127.8	100.0	W14_07_2020	40°25′854″	21°56′878″	Elafakia	46.6	18.0
W13_10_2018e	40°27′103″	21°57′639″	Potistis	110.7	90.0	W14_09_2020	40°25′854″	21°56′878″	Elafakia	48.0	33.0
W13_11_2018	40°27′103″	21°57′639″	Potistis	127.5	100.0	S10_11_2014	40°26′854″	21°58′711″	Agio Pnevma	47.8	36.7
W13_04_2019	40°27′103″	21°57′639″	Potistis	89.2	89.0	S15_06_2018	40°26′689″	21°58′801″	Agio Pnevma	15.9	15.2
W13_05_2019	40°27′103″	21°57′639″	Potistis	92.8	90.0	S10_06_2018	40°26′854″	21°58′711″	Agio Pnevma	18.5	15.6
W13_06_2019	40°27′103″	21°57′639″	Potistis	98.1	89.0	S16_07_2018	40°27′338″	21°58′750″	Agio Pnevma	2.4	1.8
W13_08_2019	40°27′103″	21°57′639″	Potistis	103.3	88.0	S17_07_2018	40°26′856″	21°58′757″	Agio Pnevma	3.8	1.5
W13_10_2019	40°27′103″	21°57′639″	Potistis	103.5	92.0	S18_07_2018	40°27′871″	21°58′475″	Agio Pnevma	2.2	1.6
W13_11_2019	40°27′103″	21°57′639″	Potistis	105.8	99.0	S19_07_2018	40°27′095″	21°58′711″	Agio Pnevma	0.5	0.5
W13_02_2020	40°27′103″	21°57′639″	Potistis	95.7	87.0	S2_03_2014	40°25′789″	21°56′216″	Mouratidis	38.3	33.9
W13_06_2020	40°27′103″	21°57′639″	Potistis	99.0	97.0	S2_09_2016	40°25′789″	21°56′216″	Mouratidis	17.0	13.0
W13_07_2020	40°27′103″	21°57′639″	Potistis	99.6	82.0	S2_02_2017	40°25′789″	21°56′216″	Mouratidis	10.0	7.00
W13_09_2020	40°27′103″	21°57′639″	Potistis	103.9	88.0	S2_04_2017	40°25′789″	21°56′216″	Mouratidis	15.0	12.0
W13_10_2020	40°27′103″	21°57′639″	Potistis	103.5	92.0	S2_05_2017	40°25′789″	21°56′216″	Mouratidis	28.0	23.0
W14_11_2014	40°25′854″	21°56′878″	Elafakia	53.5	51.1	S2_06_2017	40°25′789″	21°56′216″	Mouratidis	25.0	22.0
W14_07_2014	40°25′854″	21°56′878″	Elafakia	57.4	51.2	S2_07_2017	40°25′789″	21°56′216″	Mouratidis	26.0	19.0
W14_12_2015	40°25′854″	21°56′878″	Elafakia	52.5	49.1	S2_08_2017a	40°25′789″	21°56′216″	Mouratidis	12.0	8.00
W14_09_2016	40°25′854″	21°56′878″	Elafakia	26.0	23.0	S2_08_2017b	40°25′789″	21°56′216″	Mouratidis	23.7	21.4
W14_04_2017	40°25′854″	21°56′878″	Elafakia	42.0	41.0	S2_09_2017	40°25′789″	21°56′216″	Mouratidis	16.0	10.0
W14_05_2017	40°25′854″	21°56′878″	Elafakia	47.3	47.0	S1_03_2014	40°25′224″	21°55′889″	Agios Dimitrios	16.6	16.5
W14_06_2017	40°25′854″	21°56′878″	Elafakia	49.0	47.0	S1_08_2017	40°25′224″	21°55′889″	Agios Dimitrios	10.9	8.70
W14_08_2017	40°25′854″	21°56′878″	Elafakia	49.2	46.8	S13_06_2017	40°25′810″	21°56′900″	Agios Panteleimonas	1.50	1.00
W14_10_2017	40°25′854″	21°56′878″	Elafakia	45.4	35.2	S14_06_2017	40°25′801″	21°57′099″	Agios Panteleimonas	1.90	1.00
W14_07_2018	40°25′854″	21°56′878″	Elafakia	45.0	40.0	W21_08_2019	40°25′842″	21°56′856″	Agios Panteleimonas	18.0	7.2
W14_08_2018	40°25′854″	21°56′878″	Elafakia	49.2	42.0	S5_07_2014	40°25′713″	21°56′725″	Vazelonas	0.50	0.10
W14_10_2018	40°25′854″	21°56′878″	Elafakia	45.4	41.0	S6_07_2014	40°25′840″	21°56′882″	Vazelonas	0.80	0.50

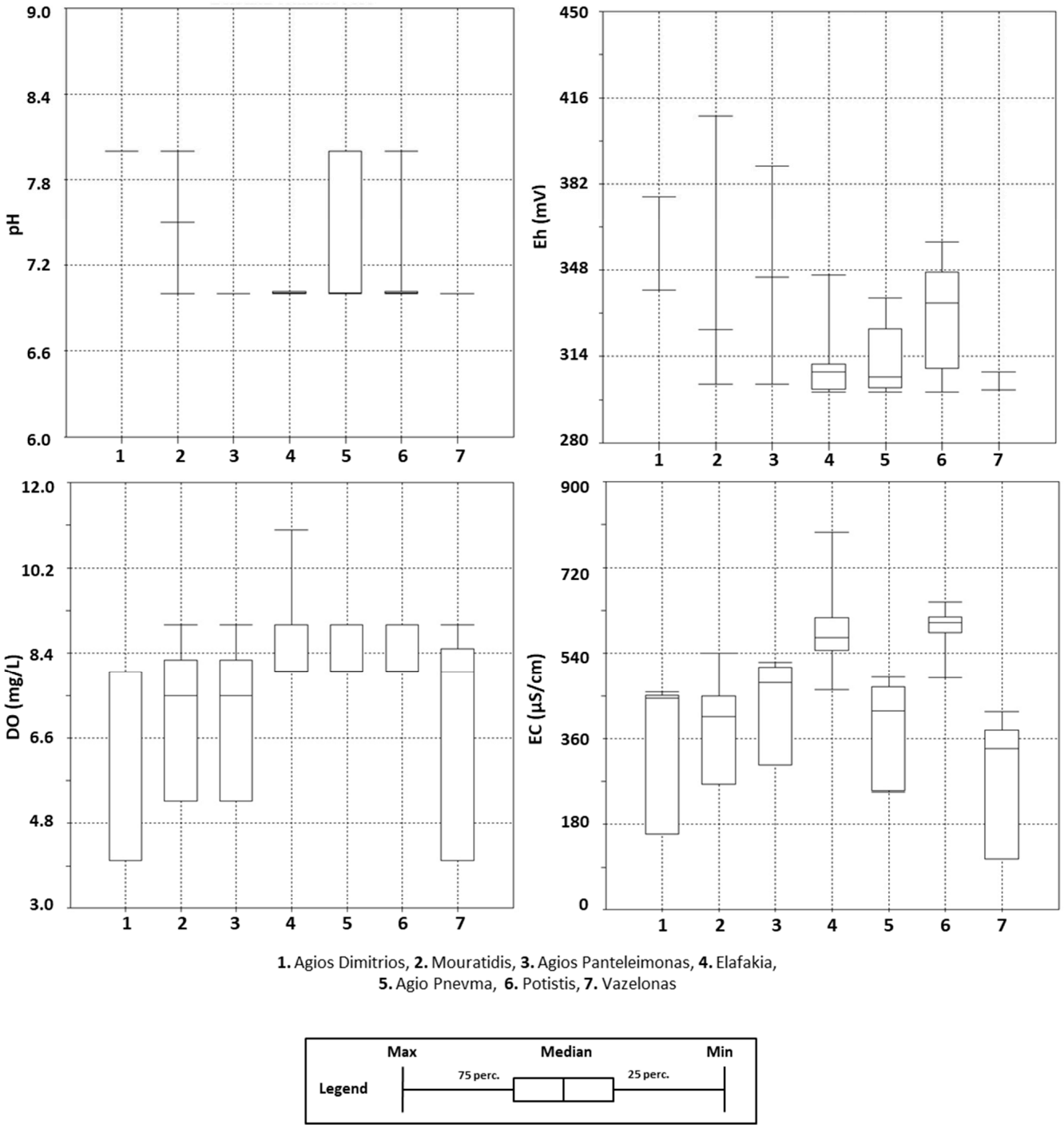

Figure 6. Box plots for the physical parameters of the natural springs of western Vermio Mt.

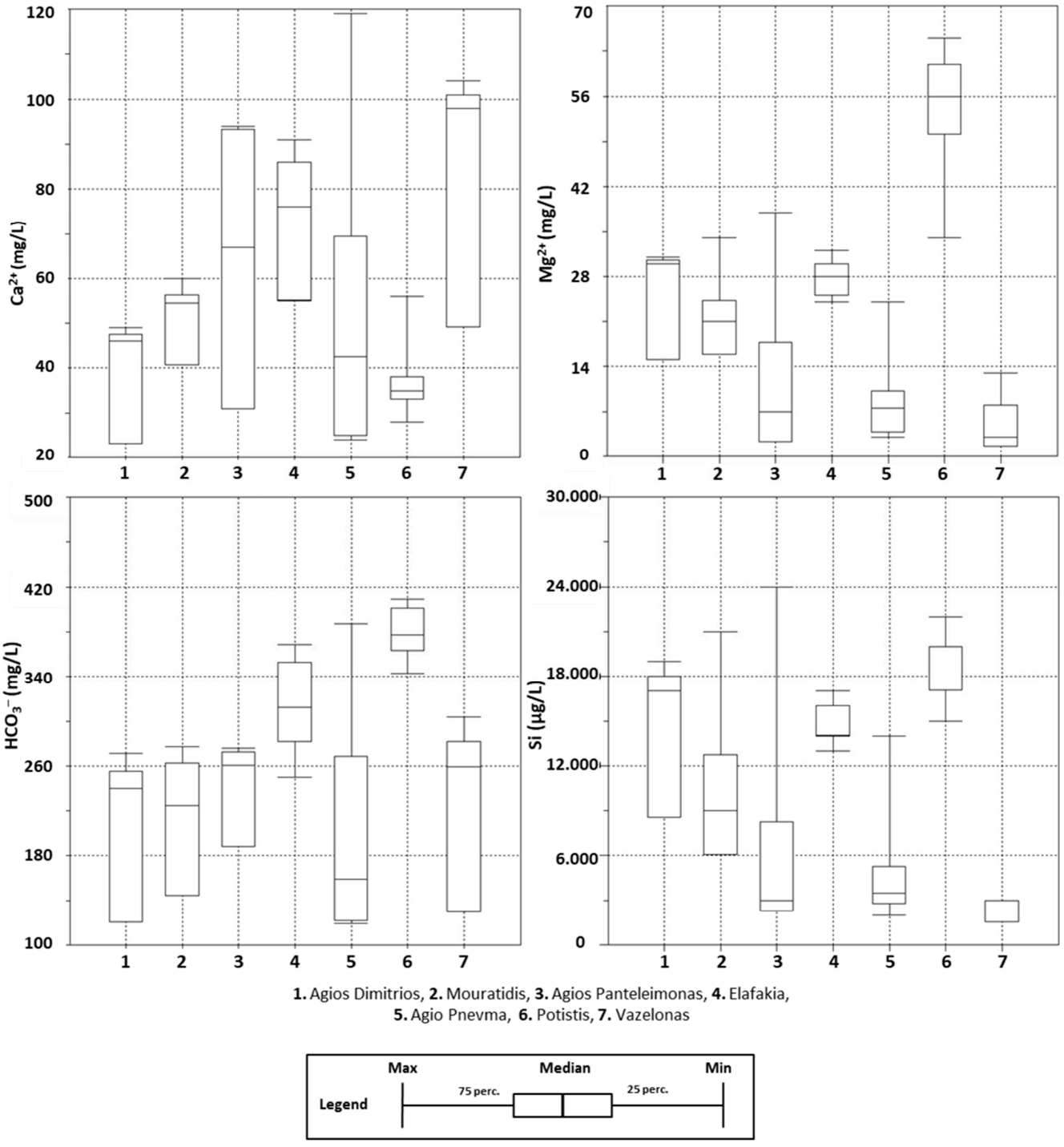

Figure 7. Box plots for the major ions and Si of the natural springs of western Vermio Mt.

Table 4. The abundance of major ions among the natural springs in western Vermio Mt.

	Area/Sampling Site	Sample ID	Cations Order	Anions Order
1	Agios Dimitrios area	S1	$Ca^{2+} > Mg^{2+} > K^{+} > Na^{+}$	$HCO_3^{-} > SO_4^{2-} > Cl^{-} > NO_3^{-}$
2	Elafakia	W14	$Ca^{2+} > Mg^{2+} > Na^{+} > K^{+}$	$HCO_3^{-} > SO_4^{2-} > Cl^{-} > NO_3^{-}$
3	Agios Panteleimonas area	S2, S13, S14	$Ca^{2+} > Mg^{2+} > Na^{+} > K^{+}$	$HCO_3^{-} > SO_4^{2-}$
4	Potistis	W13	$Mg^{2+} > Ca^{2+} > K^{+}$	$HCO_3^{-} > SO_4^{2-} > Cl^{-} > NO_3^{-}$
5	Agio Pnevma area	S18, S16, S19, S10, S17, S15	$Ca^{2+} > Mg^{2+} > K^{+} > Na^{+}$	$HCO_3^{-} > SO_4^{2-} > Cl^{-}$
6	Mouratidis	S2	$Ca^{2+} > Mg^{2+} > Na^{+} > K^{+}$	$HCO_3^{-} > SO_4^{2-} > NO_3^{-} > Cl^{-}$
7	Vazelona area	S5, S6	$Ca^{2+} > Mg^{2+} > K^{+} > Na^{+}$	$HCO_3^{-} > SO_4^{2-} > Cl^{-}$

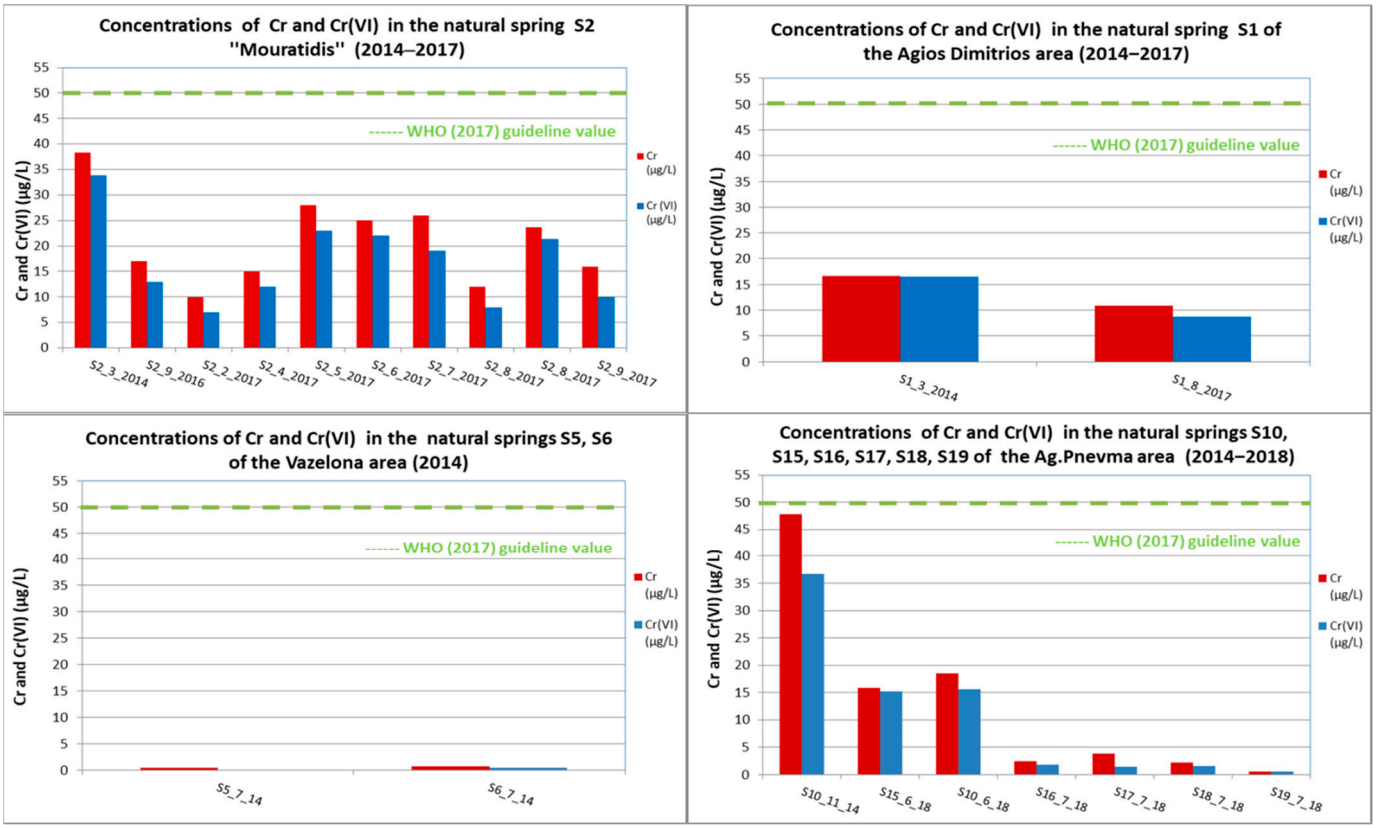

Figure 8. Concentrations of Cr and Cr(VI) in the natural springs of western Vermio Mt.

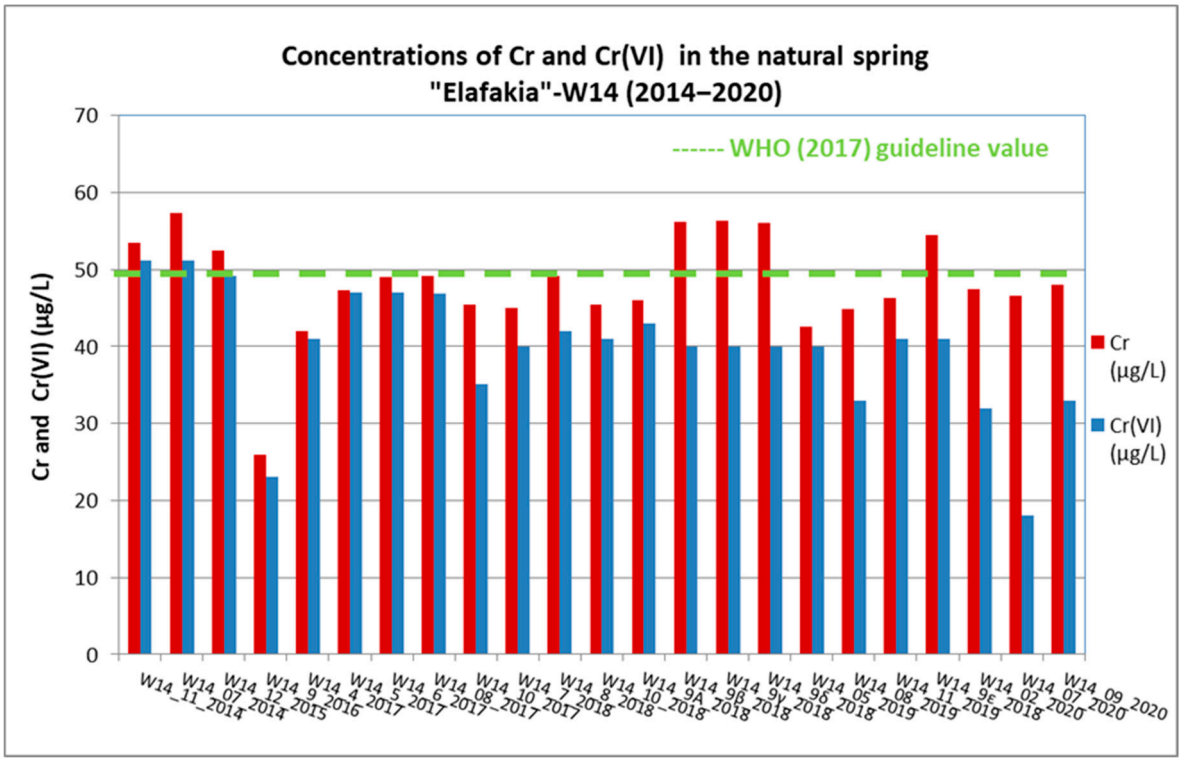

Figure 9. Concentrations of Cr and Cr(VI) in the natural spring "Elafakia"-W14 of western Vermio Mt.

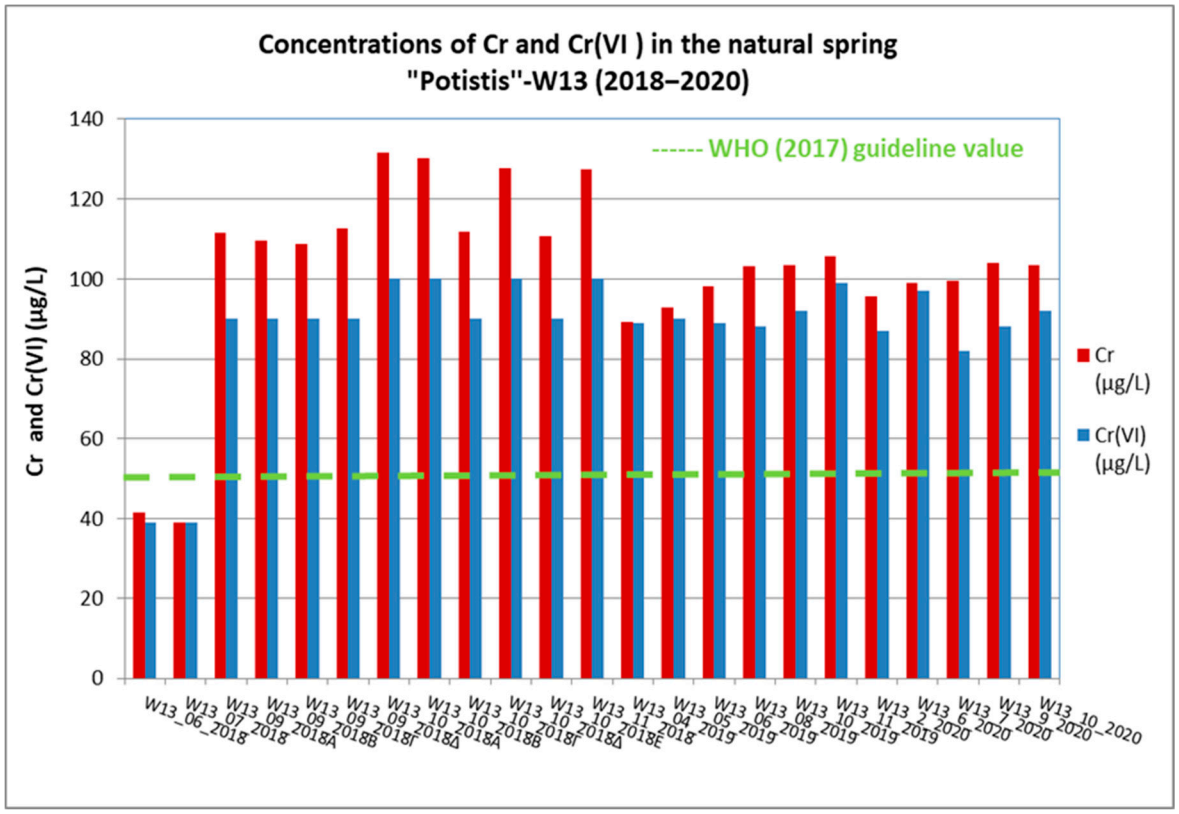

Figure 10. Concentrations of Cr and Cr(VI) in the natural spring "Potistis"-W13 of western Vermio Mt.

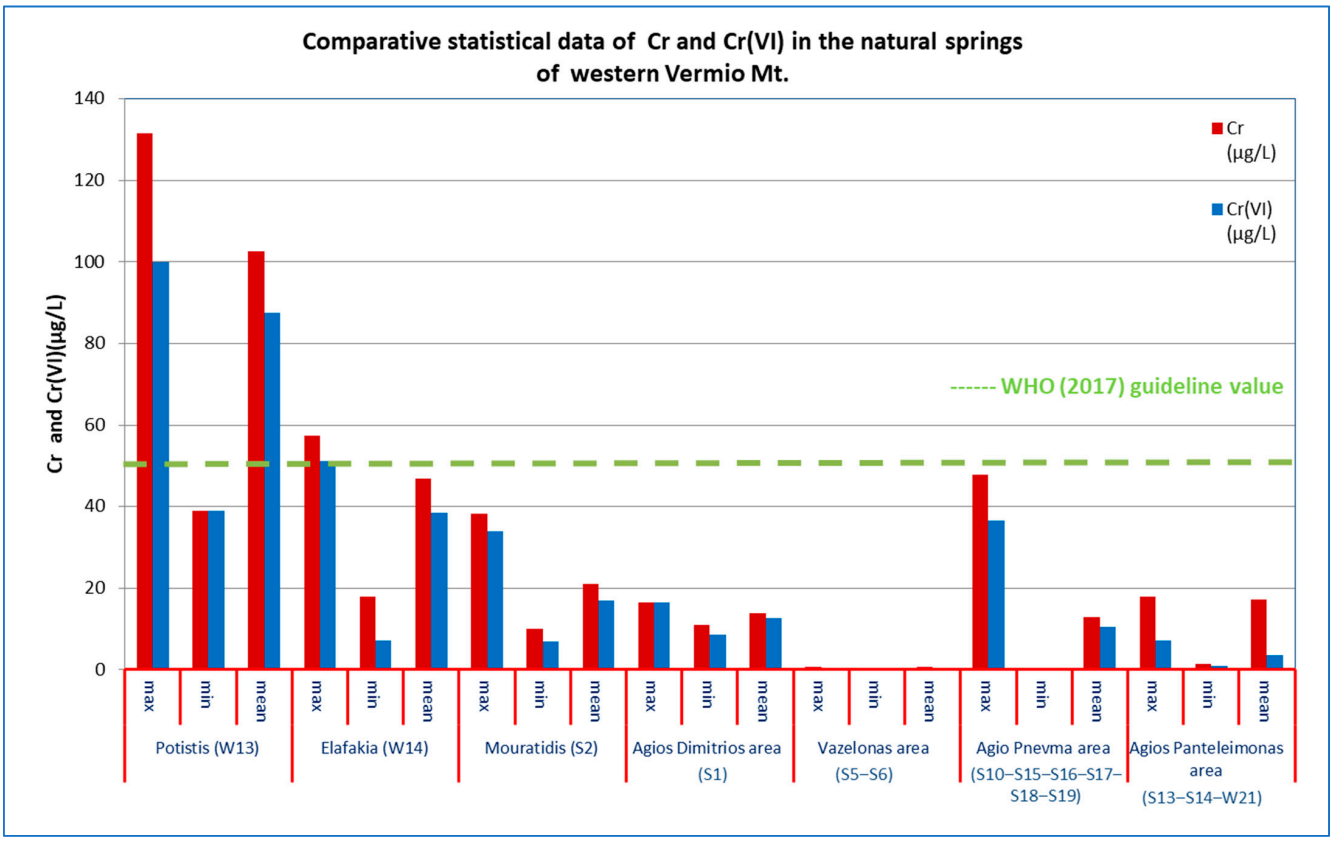

Figure 11. Statistical analyses of concentrations of Cr and Cr(VI) of the natural springs in western Vermio Mt.

3.2. Correlation Analysis of Water Samples

Spearman's rank correlation coefficient was applied to selected parameters (Table 5); the rest of the measured parameters were excluded because most of their values were BDL. The most remarkable features of the Spearman's rank correlation coefficients are the following: Cr presented a statistically significant ($p < 0.01$) very strong positive correlation coefficient with Cr(VI) ($r_s = 0.98$), strong positive correlation coefficients with Mg^{2+} ($r_s = 0.76$), Si ($r_s = 0.75$), EC ($r_s = 0.71$) and Ni (0.61), and moderate positive correlation coefficients with HCO_3^- ($r_s = 0.55$) and alkalinity ($r_s = 0.55$). Hexavalent chromium exhibited a statistically significant ($p < 0.01$) very strong positive correlation coefficient with Mg^{2+} ($r_s = 0.8$), a strong positive correlation coefficient with Si ($r_s = 0.76$) and Ni ($r_s = 0.67$), and moderate positive correlation coefficients with HCO_3^- ($r_s = 0.59$) and alkalinity ($r_s = 0.59$). Magnesium exhibited a statistically significant ($p < 0.01$) strong positive correlation coefficients with EC ($r_s = 0.68$), HCO_3^- ($r_s = 0.68$), alkalinity ($r_s = 0.68$) and Ni ($r_s = 0.60$), while very strong correlation coefficient with Si ($r_s = 0.91$). Bicarbonates presented a statistically significant ($p < 0.01$) strong positive correlation coefficient with EC ($r_s = 0.62$), and moderate positive correlation coefficients with Ni ($r_s = 0.51$), Si ($r_s = 0.48$). Sulfates had a statistically significant ($p < 0.01$) very strong positive correlation coefficient with U ($r_s = 0.82$), strong positive correlation coefficients with Sr ($r_s = 0.74$), Br ($r_s = 0.70$), Ba ($r_s = 0.63$), and Ca^{2+} ($r_s = 0.67$), and a moderate positive correlation coefficient with Na^+ ($r_s = 0.52$). Arsenic exhibited statistically significant ($p < 0.01$) strong positive correlation coefficients with U ($r_s = 0.72$), Ba ($r_s = 0.67$) and V ($r_s = 0.70$), and a moderate positive correlation coefficient with K^+ ($r_s = 0.49$).

Table 5. Spearman's rank correlation matrix of selected major and trace elements of the natural springs of western Vermio Mt.

Parameter	pH	DO	EC	Eh	Ca^{2+}	Mg^{2+}	Na^{+}	K^{+}	NO_3^{-}	Cl^{-}	SO_4^{2-}	HCO_3^{-}	Al	As	B	Ba	Br	Cr	Cr(VI)	Li	Mn	Ni	P	Si	Sr	U	V	Zn	Alkalinity
pH	**1**																												
DO	−0.11	**1**																											
EC	−0.15	0.21	**1**																										
Eh	−0.11	0.06	0.19	**1**																									
Ca^{2+}	−0.18	0.10	−0.20	0.15	**1**																								
Mg^{2+}	0.06	0.05	0.68 **	0.32	−0.42 *	**1**																							
Na^{+}	−0.17	−0.06	−0.16	−0.15	0.49 **	−0.18	**1**																						
K^{+}	0.12	−0.27	−0.28	−0.06	0.51**	−0.511 **	0.13	**1**																					
NO_3^{-}	0.18	−0.04	−0.41 *	0.13	0.31	−0.18	0.47 **	0.03	**1**																				
Cl^{-}	−0.04	−0.15	−0.30	−0.43	0.29	−0.461 **	0.37 *	0.39 *	0.19	**1**																			
SO_4^{2-}	−0.06	−0.07	0.09	−0.08	0.67 **	−0.21	0.52 **	0.49 **	0.20	0.25	**1**																		
HCO_3^{-}	−0.11	0.04	0.62 **	0.14	0.00	0.68 **	−0.15	−0.31	−0.22	−0.14	0.01	**1**																	
Al	0.17	0.10	−0.40 *	−0.24	−0.07	−0.08	0.09	−0.03	0.18	0.28	−0.14	−0.19	**1**																
As	0.17	−0.20	−0.10	0.19	0.42 *	0.00	0.51**	0.49 **	0.33	−0.04	0.60 **	−0.25	0.09	**1**															
B	−0.11	0.31	0.39 *	0.25	0.19	0.37 *	0.04	0.00	0.20	−0.19	0.25	0.41 *	−0.14	0.18	**1**														
Ba	−0.01	0.04	0.18	0.04	0.47 **	0.14	0.26	0.41 *	0.12	−0.10	0.63 **	0.18	0.06	0.67 **	0.45 **	**1**													
Br	−0.17	0.10	0.28	−0.22	0.33	−0.02	0.32	0.21	0.04	0.31	0.70 **	0.21	−0.05	0.20	0.26	0.45 **	**1**												
Cr	−0.11	0.32	**0.71** **	0.19	−0.30	**0.76** **	−0.09	−0.55 **	−0.19	−0.33	−0.13	**0.55** **	−0.12	−0.16	0.38 *	0.07	0.17	**1**											
Cr(VI)	−0.14	0.32	**0.73** **	0.18	−0.34	**0.80** **	−0.10	−0.6 **	−0.19	−0.35 *	−0.17	**0.59** **	−0.09	−0.19	**0.36 ***	0.06	0.17	**0.98** **	**1**										
Li	0.17	0.04	0.42 *	0.13	−0.17	0.611 **	−0.08	0.05	−0.15	−0.32	0.23	0.22	0.11	0.48 **	0.39 *	0.63 **	0.29	**0.47** **	0.48 **	**1**									
Mn	0.17	−0.26	−0.30	−0.44 *	−0.15	−0.19	−0.13	0.04	0.05	0.06	−0.07	−0.11	0.30	−0.04	−0.43	−0.05	−0.09	−0.41 *	−0.32	−0.14	**1**								
Ni	−0.27	0.30	0.60 **	0.07	−0.13	0.60**	−0.10	−0.25	−0.25	−0.30	0.01	0.51 **	0.10	0.04	0.42 *	0.45 **	0.37*	**0.61** **	0.67 **	0.64 **	−0.10	**1**							
P	−0.09	−0.07	−0.27	−0.41 *	−0.08	−0.28	−0.15	−0.02	−0.03	0.10	−0.07	0.00	0.25	−0.23	−0.30	−0.13	−0.04	−0.36 *	−0.26	−0.24	0.75 **	−0.04	**1**						
Si	0.10	−0.07	0.58 **	0.34	−0.43 *	0.91 **	−0.20	−0.34	−0.11	−0.43 *	−0.19	0.48 **	−0.07	0.09	0.34	0.17	−0.09	**0.75** **	0.76 **	0.71 **	−0.22	**0.53** **	−0.33	**1**					
Sr	−0.13	0.01	−0.26	−0.18	0.827 **	−0.55	0.61 **	0.61 **	0.21	0.38 *	0.74 **	−0.23	0.06	0.53 **	0.12	0.56 **	0.47 **	−0.37 *	−0.43	−0.04	−0.09	−0.13	−0.07	−0.53	**1**				

Table 5. *Cont.*

Parameter	pH	DO	EC	Eh	Ca^{2+}	Mg^{2+}	Na^{+}	K^{+}	NO_3^{-}	Cl^{-}	SO_4^{2-}	HCO_3^{-}	Al	As	B	Ba	Br	Cr	Cr(VI)	Li	Mn	Ni	P	Si	Sr	U	V	Zn	Alkalinity
U	−0.14	0.12	−0.03	−0.09	0.676 **	−0.27	0.59 **	0.462 **	0.28	0.15	0.82 **	−0.15	0.05	0.72 **	0.33	0.78 **	0.58 **	−0.16	−0.18	0.29	−0.05	0.18	−0.03	−0.28	0.85 **	**1**			
V	0.10	0.02	−0.08	0.08	0.15	0.16	0.30	0.16	0.33	−0.11	0.41 *	−0.13	0.25	0.70 **	0.21	0.69 **	0.19	−0.10	−0.09	0.59 **	0.07	0.26	−0.07	0.22	0.24	0.54 **	**1**		
Zn	−0.01	−0.10	−0.50 **	−0.23	0.22	−0.33	0.24	0.18	0.52 **	0.38 *	0.04	−0.22	0.32	0.09	−0.05	0.09	−0.04	−0.23	−0.22	−0.18	0.34	−0.16	0.41 *	−0.24	0.23	0.21	0.09	**1**	
Alkalinity	−0.11	0.04	0.62 **	0.14	0.00	**0.68** **	−0.15	−0.31	−0.22	−0.14	0.02	1 **	−0.19	−0.24	0.41 *	0.19	0.22	**0.55** **	**0.59** **	0.23	−0.11	**0.50** **	0.00	0.48 **	−0.22	−0.14	−0.13	−0.22	**1**

* Correlation is significant at the 0.05 level (2-tailed). ** Correlation is significant at the 0.01 level (2-tailed).

4. Discussion

4.1. Hydrogeochemical Characterization of the Natural Springs of Western Vermio Mt. the Ultramafic Fingerprint

The dominant hydrochemical types of the studied natural springs of western Vermio Mt. were Ca-Mg-HCO_3 (40% of the water samples), Mg-Ca-HCO_3 (33% of the water samples), and Ca-HCO_3 (21%) (Figure 12). Other transitional water types in the study area comprised Ca-K-HCO_3-Cl (3%) and Ca-HCO_3-SO_4 (3%). Based on the type and the geological environment of the springs, the Ca–HCO_3 waters are considered to originate through the interaction of meteoric water with rocks containing Ca-bearing minerals, whereas water types enriched in Mg, were derived from the dissolution of ultramafic rocks [29]. The mixed Ca-Mg-HCO_3 type indicated fresh recharge waters mainly related to carbonate rocks and less to ultramafic rocks. The Mg-Ca-HCO_3 water type represents recharge waters related to Mg-rich rocks, suggesting the strong interaction with the ultramafic rocks of the area [67]. The springs "Potistis"-W13, S1, and W21 that belong to this type are associated with fissured aquifers in strongly serpentinised ultramafic rocks, or they are in hydraulic connection with them.

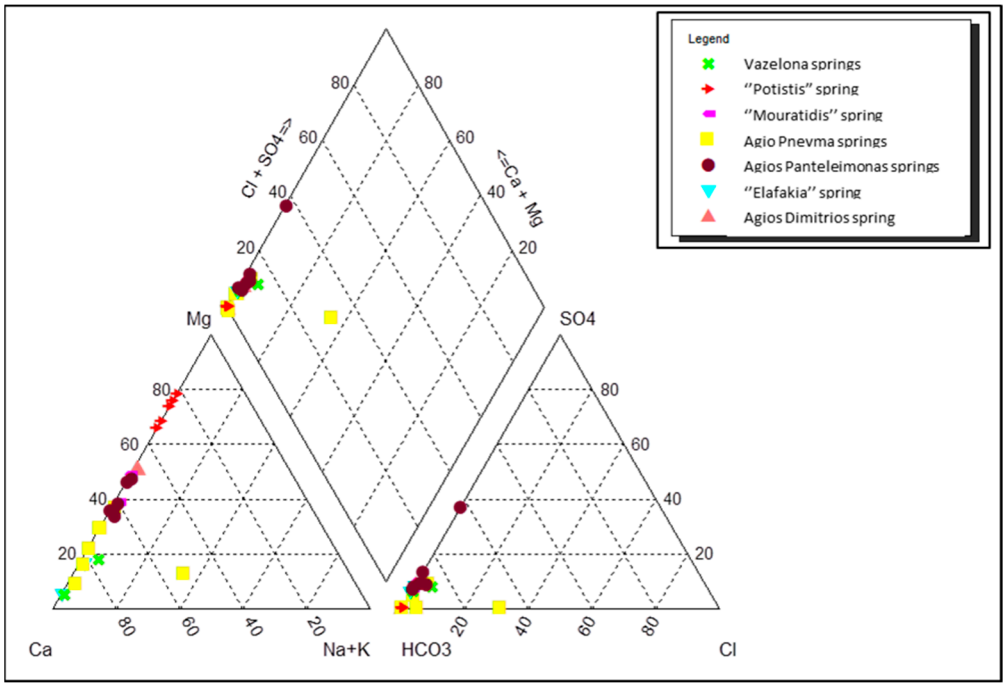

Figure 12. Piper diagram of major ion chemistry for the natural spring samples.

The water–ultramafic rock interaction typically produces Mg-HCO_3 water type [33,40,68] and slightly alkaline to strongly alkaline pH conditions [69] because of the absorption of dissolved CO_2 from atmospheric water in the serpentine and olivine according to the Equations (6) and (7) [70]:

$$Mg_3Si_2O_5(OH)_4 + 6CO_2 + 5H_2O \rightarrow 3Mg^{2+} + 6HCO_3^- + 2H_4SiO_4 \quad (6)$$

$$Mg_2SiO_4 + 4H_2O + 4CO_2 \rightarrow 2Mg^{2+} + 4HCO_3^- + H_4SiO_4 \quad (7)$$

The pH values that characterised the studied springs varied from 7.3 up to 8.5, indicating near-neutral to slightly alkaline conditions that are typical of groundwater interacting with ultramafic and carbonate rocks [40,71]. Redox potential conditions were oxidizing up to strong oxidizing, as indicated by Eh, ranging from 300 mV up to 410 mV. The pH and Eh conditions in the studied springs favoured the release and solubility of the Cr oxyanion in groundwater since the solubility of oxyanions such as $HCrO_4^-$, CrO_4^{2-}, $Cr_2O_7^{2-}$, $H_2AsO_4^-$, and $HAsO_4^{2-}$ is enhanced with increasing pH [72].

Various tools are usually employed to define and evaluate the water–rock interaction processes in an area [73]. Bivariate plots of major ions and ionic ratios were used to study the hydrogeochemical evolution processes in the studied springs (Figure 13). In the bivariate plot of Ca vs. Mg, the water samples were grouped into three classes based on their Ca/Mg ratio (Figure 13a). In the first class belong the water samples with a Ca/Mg ratio below the 1:3 line. This class included two seasonal water samples from the spring "Potistis"-W13 (W13_10_19 and W13_4_19) with a Mg-Ca-HCO_3 water type, revealing that the flow path was mainly through serpentinites. The second class contained the water samples of the natural spring S1-Agios Dimitrios area and "Potistis"-W13. They are all of Mg-Ca-HCO_3 type and characterized by Ca/Mg ratios plotted below the 1:1 and above the 1:3 lines; this suggests a mixture of Mg-HCO_3 and Ca-HCO_3, indicating that these waters were derived from interaction with serpentinites and Ca-rich rocks. The third class comprised the rest of natural springs, characterized by mixed water types and a Ca/Mg ratio above the 1:1 line, indicating a limited influence of serpentinites. The bivariate plot of Ca + Mg vs. HCO_3 (Figure 13b) suggests an excess of (Ca + Mg) over HCO_3 reflecting an additional non-carbonate source of Ca^{2+} and Mg^{2+} ions, such as the dissolution of silicate minerals [38,57]. Iron-Mg-silicates of ultramafic rocks, such as olivine, pyroxene, and amphibole are transformed to serpentine group minerals during the serpentinisation process. Dissolution reactions favour the Mg^{2+} and HCO_3^- release of the Mg-rich minerals (Equations (6) and (7)) [68].

During water–rock interaction, various chemical processes (e.g., fluctuation of ionic concentrations, mobilization of the dissolved components, and change in pH) are fingerprinted on the groundwater quality [74,75]. Gibbs diagrams are generally used to identify the hydrogeochemical evolution of groundwater, which involves precipitation, water–rock interaction, and evaporation–crystallization processes, based on TDS vs. $Na^+/(Na^+ + Ca^{2+})$, and TDS vs. $Cl^-/(Cl^- + HCO_3^-)$ scatter diagrams [76]. Herein, Gibbs diagrams were employed to assess hydrogeochemical processes that affect the water chemistry in the natural springs of western Vermio Mt. Figure 14 illustrates that all samples from natural springs fall into the water–rock interaction field, suggesting weathering of carbonate and silicate minerals. Although the use of Gibbs plots for groundwater has been disputed [77], the case study discussed herein exhibits none of the characteristics that could result in misuse of these plots (e.g., high SO_4^{2-} concentrations, salinity sources, evolutionary flow paths, etc.). The implications of the Gibbs diagrams are in accordance with the calculated MGI index, according to which the waters from the natural springs are characterized as deep percolation types.

4.2. Hydrogeochemistry of Cr in Natural Ultramafic Springs

To further study the hydrogeochemistry of Cr in the studied springs, the average concentration of Cr was plotted vs. the water type of each spring (Figure 15). As shown, each water type is characterised by a wide range of concentrations of Cr, attributed to the different operation mechanisms of the spring and the weathering degree of the host geological formations. The mixed Mg-Ca-HCO_3 water type ranges from very high concentrations of Cr, in the spring "Potistis"-W13 (>100 μg/L), to much lower values (<20 μg/L) in the springs S1-Agios Dimitrios area and W21-Agios Panteleimonas area. The mixed Ca-Mg-HCO_3 water type is related to a range of concentrations of Cr from 17 to 48 μg/L. On the other hand, all springs that are characterised by a Ca-HCO_3 water type exhibit very low Cr concentrations (<5 μg/L) since mostly the carbonate rocks influence their hydrochemistry. In all springs, the dominant anion is HCO_3^-, the principal source of which is the dissolution of carbonate and silicate minerals [33].

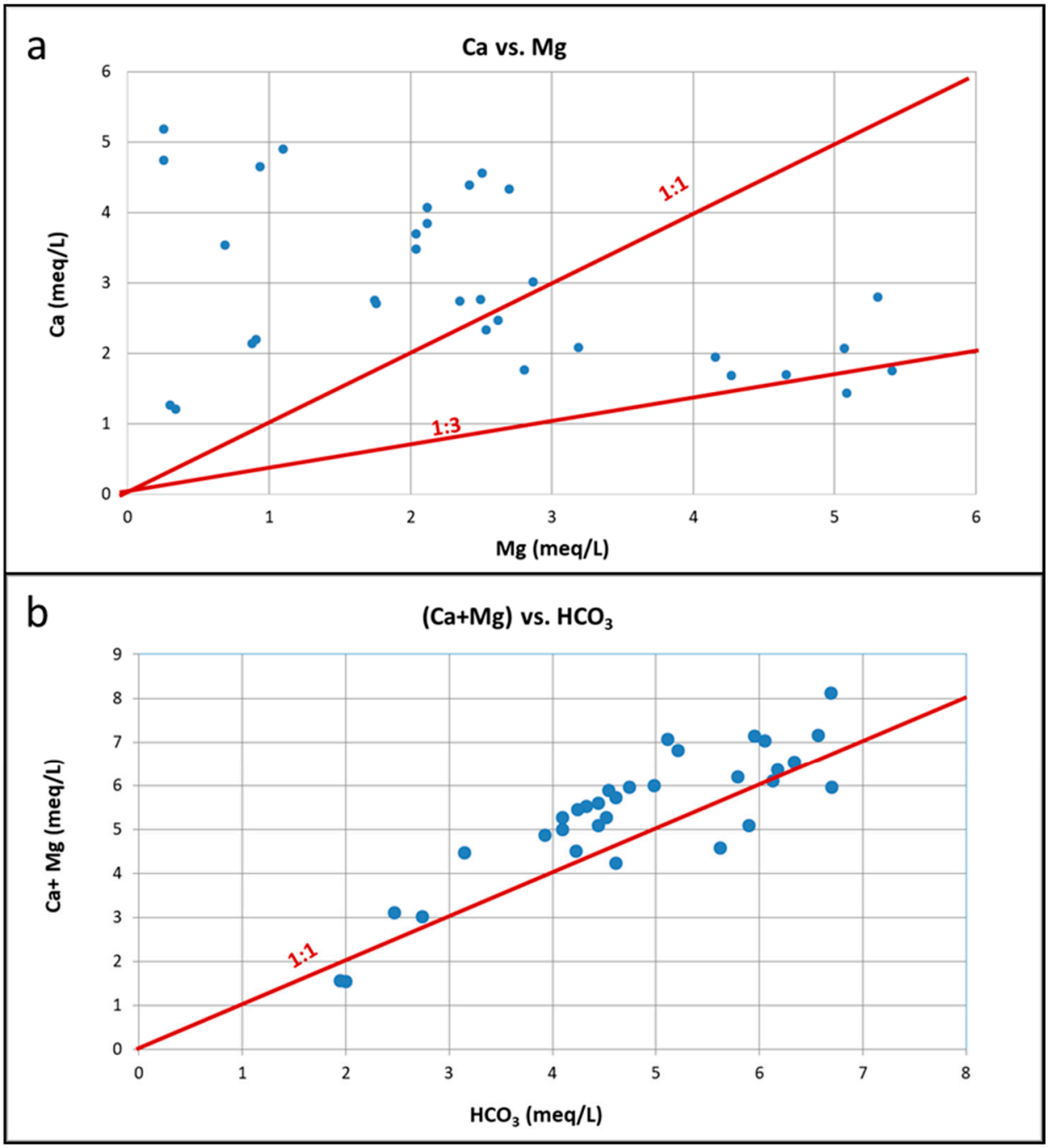

Figure 13. Bivariate plots of: (**a**) Ca vs. Mg and (**b**) (Ca+Mg) vs. HCO_3 for the natural springs of western Vermio Mt.

An interesting feature of the spring "Potistis"-W13, derived from the evaluation of hydrogeochemical, hydrological, and meteorological data, is the decrease in concentrations of Cr in a very short time after rainfall; this is further supported by the strong linear regression of Cr vs. discharge (coefficient of determination $R^2 = 0.85$) (Figures 16 and 17). Low discharge results in increased water–ultramafic rock contact time and thus, in elevated concentrations of Cr.

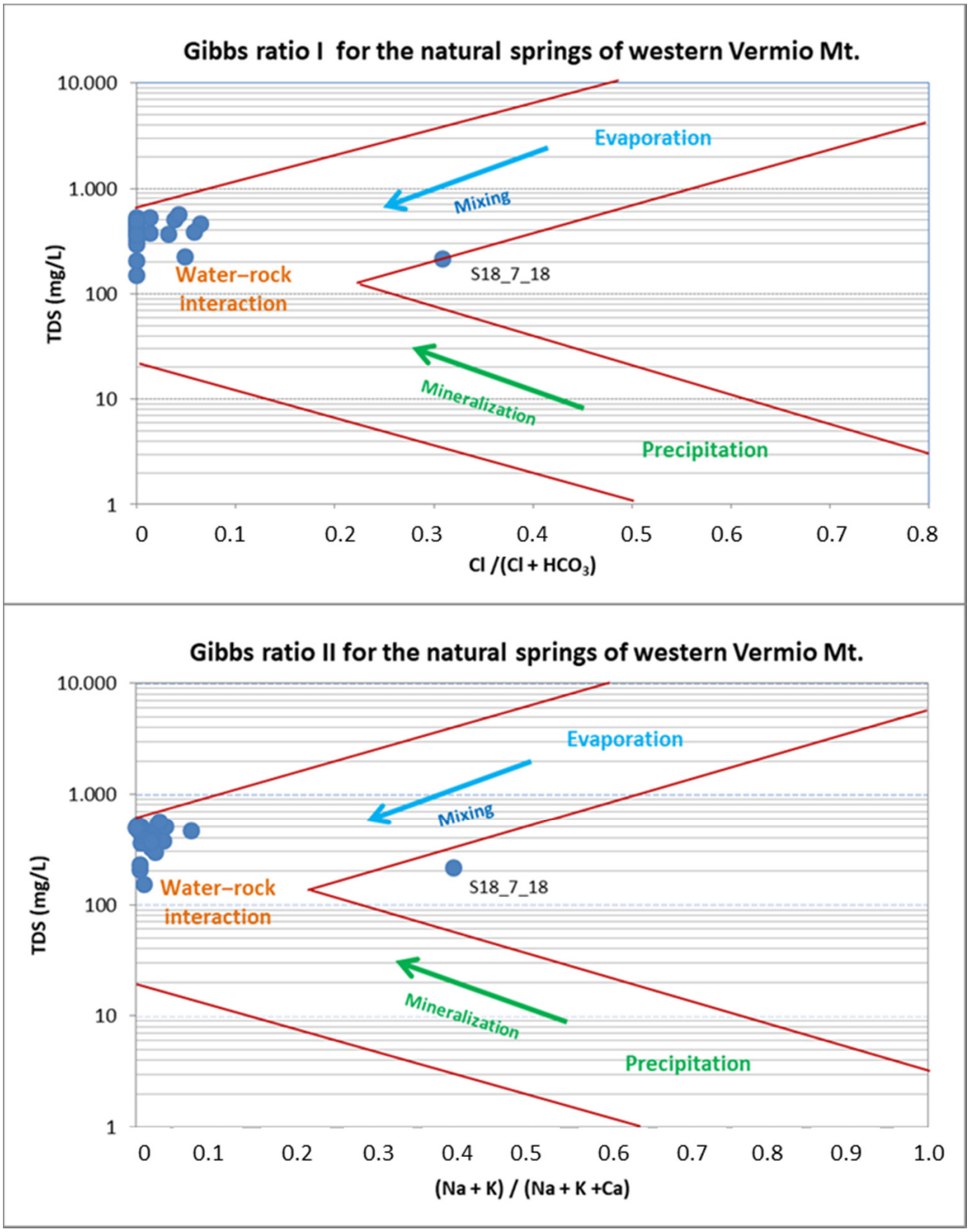

Figure 14. Gibbs diagrams of the natural springs in western Vermio Mt.

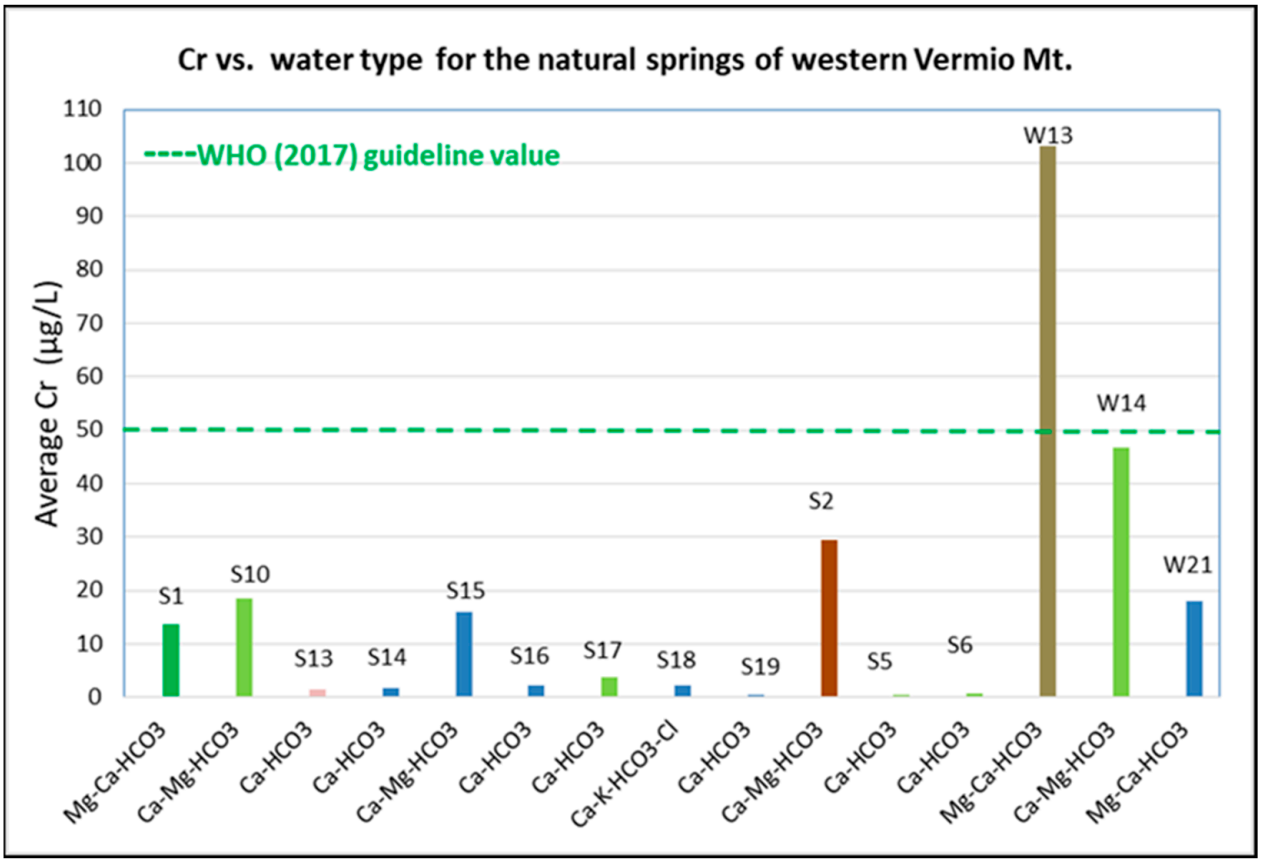

Figure 15. Average concentrations of Cr vs. water types of the natural springs in western Vermio Mt.

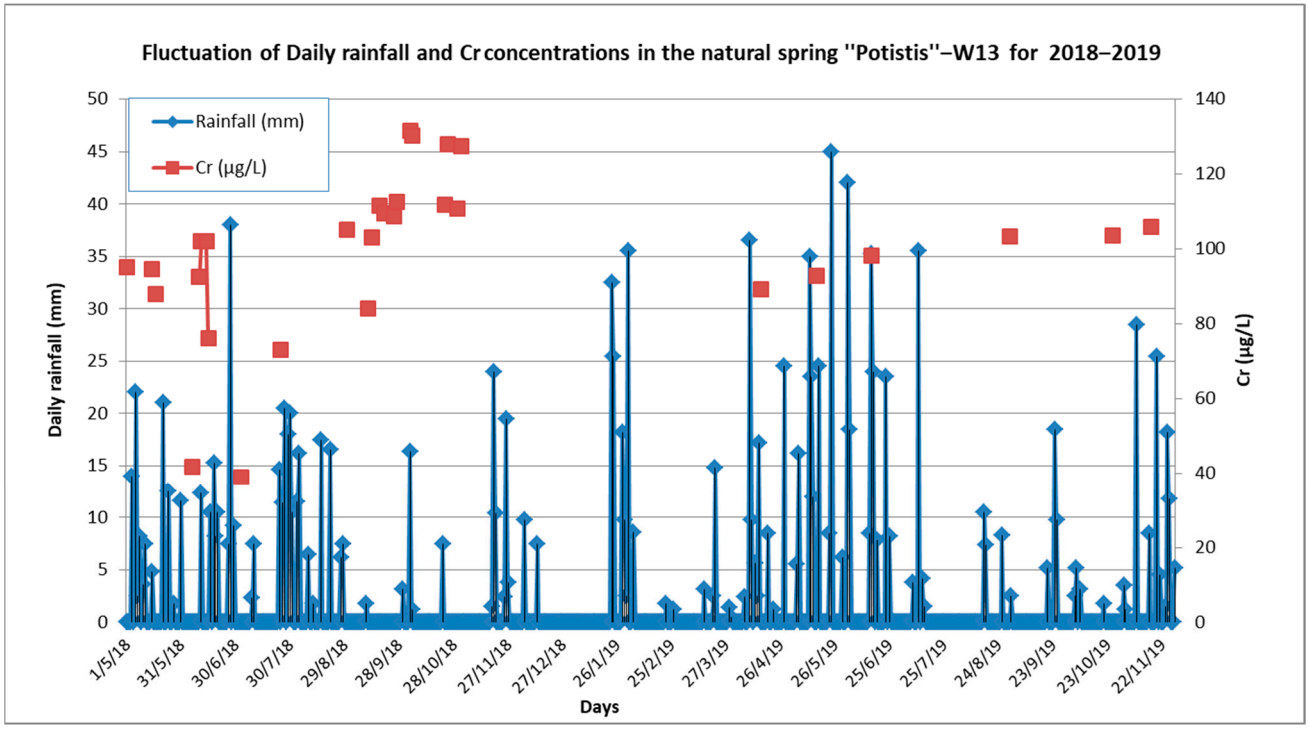

Figure 16. Fluctuation diagrams of rainfall and Cr concentrations of the natural spring "Potistis"-W13 in western Vermio Mt.

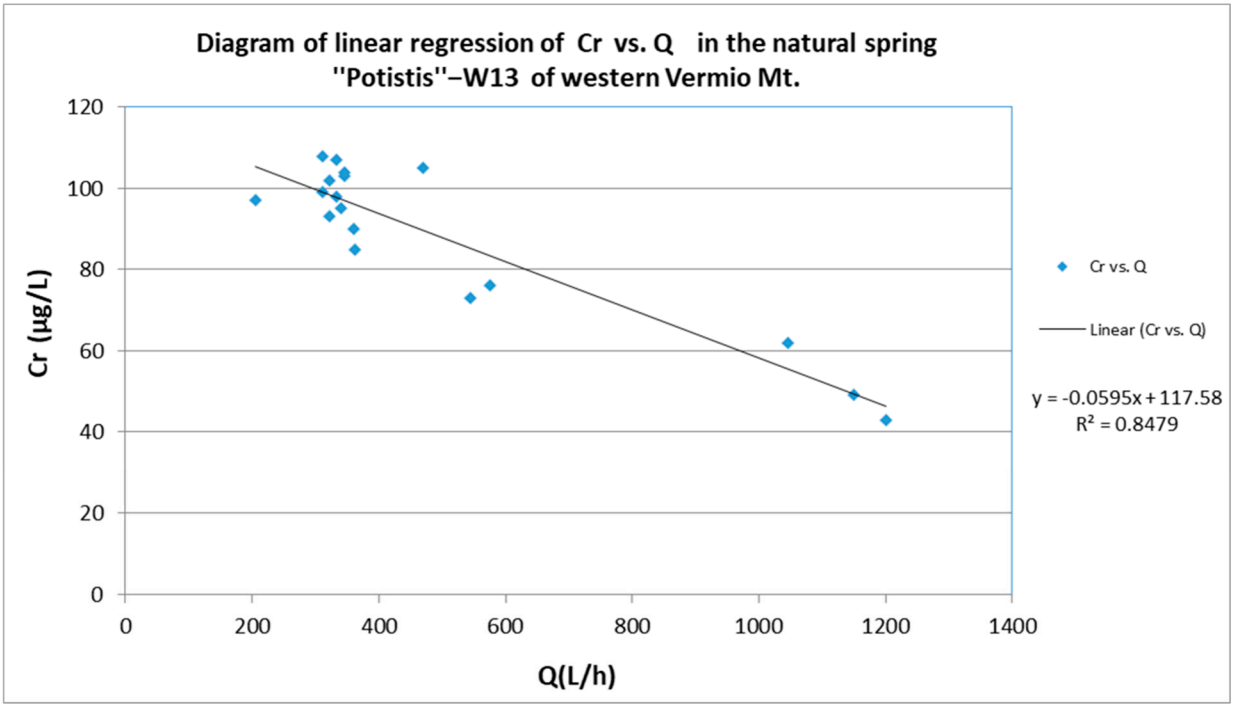

Figure 17. Plot of Cr (μg/L) vs. discharge (L/h) in the natural spring "Potistis"-W13 in western Vermio Mt.

In Figure 18a, the Mg/Si ratio vs. Cr in the springs is presented. The diagram is divided into three sub-groups according to the concentrations of Cr. The water samples with low concentrations of Cr (<30 μg/L) constituted 45.5% of the total samples, 73.3% of which exhibited a Mg/Si ratio lower than 2. Concentrations of Cr from 30 μg/L up to 50 μg/L, comprised 25% of the total water samples, 77.78% of which exhibited a Mg/Si ratio lower than 2.3; only the samples W13_6_18 and W13_7_18 which correspond to the lowest concentrations of Cr recorded in the spring "Potistis"-W13 exhibited a Mg/Si ratio higher than 2.3. Of the total water samples, 42% exceeded the permissible limit of 50 μg/L for drinking water [66], with most of them corresponding to samples from the spring "Potistis"-W13. Most samples presented a Mg/Si ratio higher than 2.3. Respective Mg/Si ratios have been reported for groundwater in other natural ultramafic environments [29,33].

The strong fingerprint of the water–rock interaction on the spring water chemistry and the geogenic origin of Cr in groundwater are indicated by the statistically significant very strong positive correlation coefficient of Cr with Si, the strong positive correlation coefficients of Cr with Mg^{2+}, EC, and Ni, and the moderate positive correlation coefficients of Cr with HCO_3 and alkalinity. Magnesium and alkalinity are two parameters usually increased with increasing degree of weathering; the latter has been reported to relate to elevated concentrations of Cr in groundwater [78]. Nickel is derived from the dissolution of Ni-bearing silicates which are released to groundwater under morphological and geochemical conditions that do not favour the occurrence of Fe-hydroxides and other secondary minerals capable of adsorbing Ni [79]. Nickel exhibited statistically significant, moderate positive correlation coefficients with Mg^{2+}, EC, and Si, further highlighting its geogenic origin. The two natural springs with high concentrations of Ni ("Potistis"-W13, "Elafakia"-W14), also exhibit high mean concentrations of dissolved Si, and are of Mg-Ca-HCO_3 and Ca-Mg-HCO_3 water type. A similar case of high concentrations of Cr and Ni in Mg-HCO_3 groundwater has been reported by Margiotta et al. [40]. Unlike the spring waters, Cr in the irrigational wells in the lowland of the Sarigkiol Basin was reported to strongly correlate with NO_3^- and P, indicating the synergistic role of the agricultural activities [45].

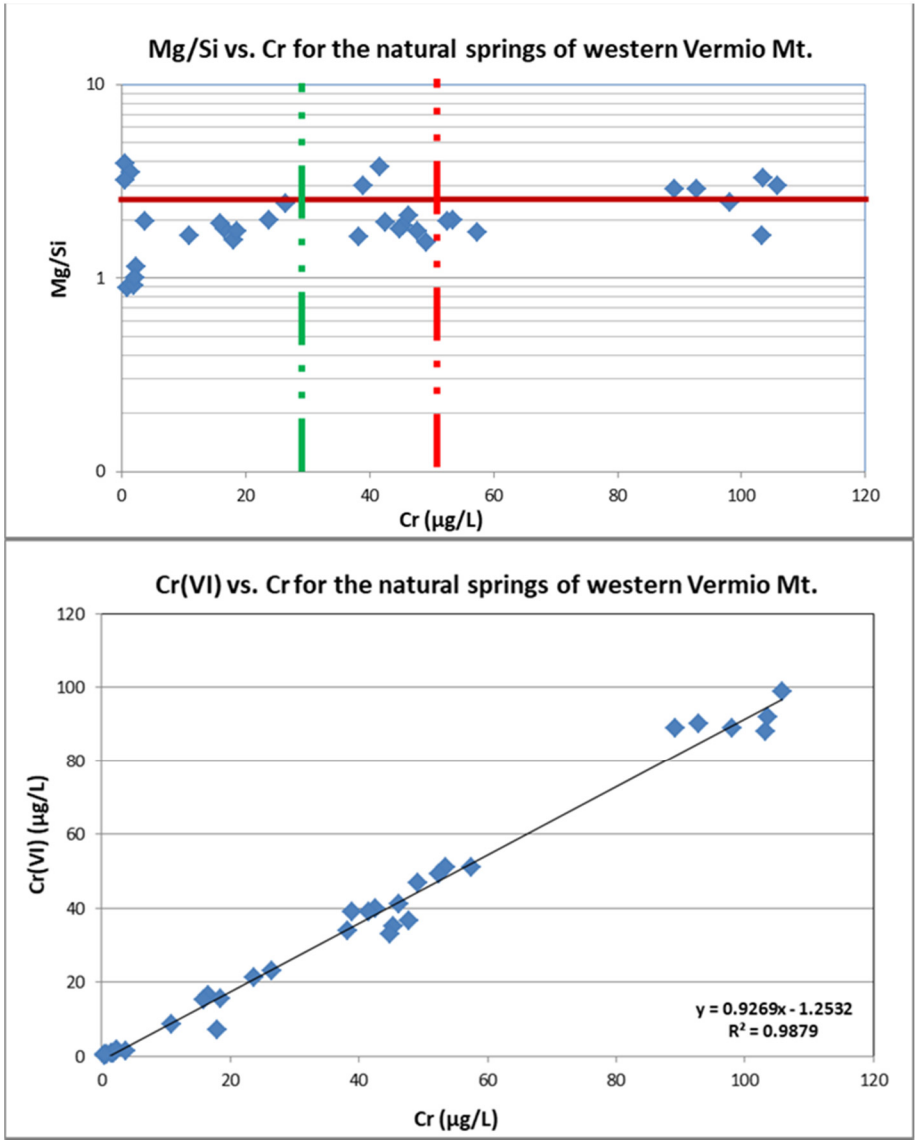

Figure 18. Plots of: (**a**) Mg/Si vs. Cr and (**b**) Cr(VI) vs. Cr (regression model) of the natural springs in western Vermio Mt.

The statistically significant, very strong positive correlation coefficients of Cr with Cr(VI) (Spearman's rank correlation coefficient r_s = 0.986) was further proven by their linear regression with a strong linear relationship (coefficient of determination R^2 = 0.99, Figure 18b). In the analysed water samples, the Cr(VI)/Cr ratio ranges from 20% up to 100%. Specifically: (a) 62.5–90.3% in the spring "Mouratidis"-S2, (b) 80–99% in the spring S1- Agios Dimitrios area, (c) 20–62.5% in the springs at the Vazelonas area, (d) 39–100% in the springs at the Agio Pnevma area, (e) 40–99% in the spring "Elafakia"-W14, (f) 76–100% in the spring "Potistis"-W13). The fluctuation in the Cr(VI)/Cr ratio depends on the prevailing geochemical conditions (redox reactions, pH), the presence of iron or manganese oxides, and competing anions in each area, suggesting that various processes take place [78]. Hexavalent chromium is the principal form of Cr in the natural water springs ("Potistis"-W13, S1-Agios Dimitrios area, "Mouratidis"-S2); several factors contribute to the high Cr(VI)/Cr ratio. Specifically, the geological environment, which is enriched in Ca and Mg-bearing minerals, enhances Cr(VI) to form complexes with Mg and Ca and inhibits Cr(VI) reduction [71]. The presence of manganese oxides enhances the Cr(III) oxidation to

Cr(VI) in ultramafic rocks, soils, and unsaturated zone releasing Cr(VI) to groundwater (Equation (8)) [24].

$$Cr(III) + 1.5\delta - MnO_{2(s)} + H_2O \rightarrow HCrO_4^- + 1.5Mn^{2+} + H^+ \quad (8)$$

The pronounced role of minerals in the concentrations of Cr in natural springs was investigated via SIs of selected mineral phases present in the study area (Figure 19). The percentage distribution of the SIs for the selected mineral phases is given in Table 6 for all collected water samples.

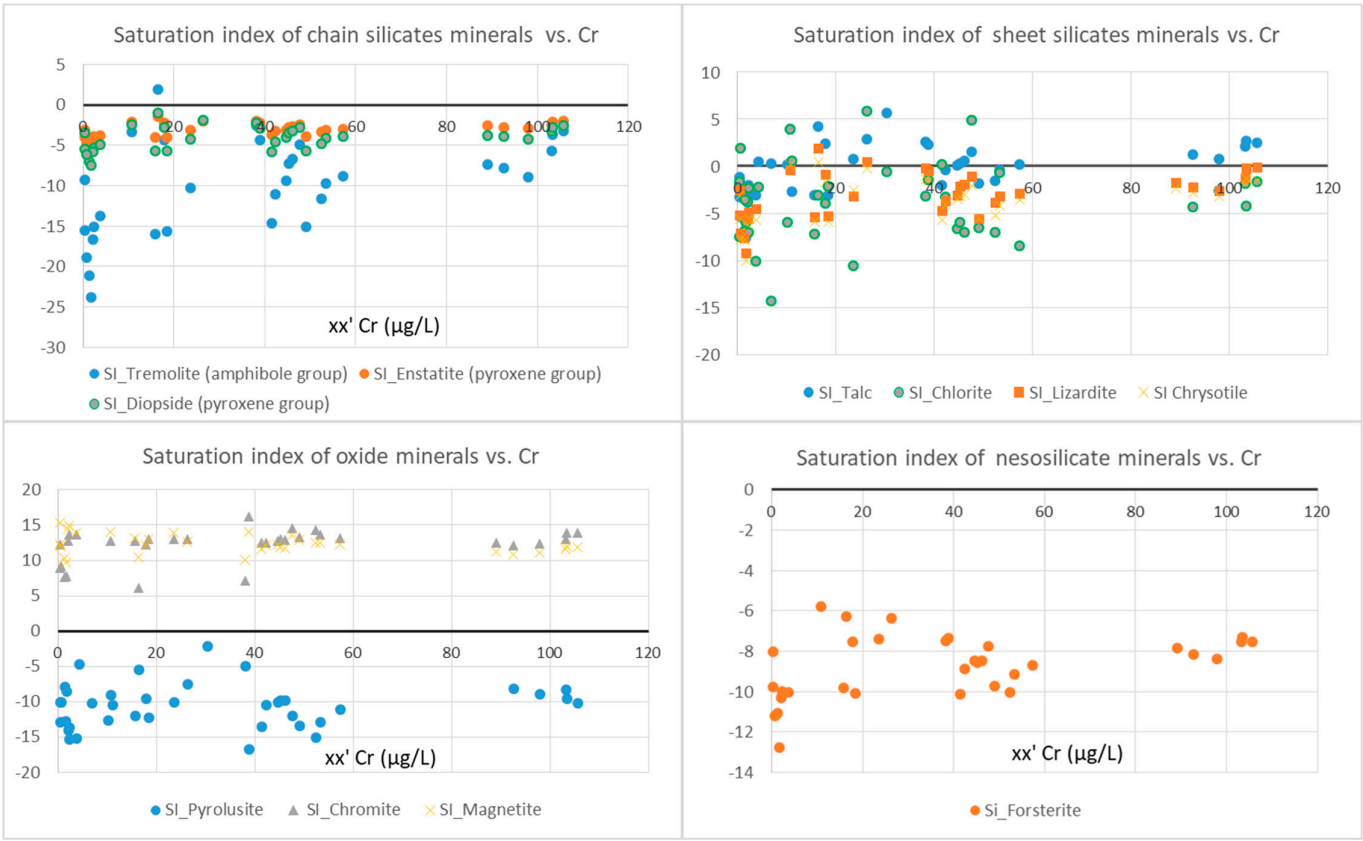

Figure 19. Plots of saturation indices vs. Cr of the natural springs in western Vermio Mt.

The water samples from the natural springs in which concentrations of Cr exceeded 50 µg/L ("Potistis"-W13 and "Elafakia"-W14) were oversaturated in: (a) the carbonate mineral calcite (100%) and (b) the oxide minerals chromite (100%) and magnetite (100%). On the other hand, they are undersaturated in: (a) the serpentine group minerals lizardite (100%) and chrysotile (100%), (b) the pyroxenes enstatite (100%) and diopside (100%), and the amphibole tremolite (100%) and (c) the olivine (100%).

In general, the mineralogical phases that appear undersaturated tend to dissolve in water. The dissolution reactions contribute major, minor elements and PTEs to the groundwater. Chromium-bearing silicate minerals (serpentine, amphibole, pyroxene, chlorite, talc) occurred mostly undersaturated in the water samples, whereas Cr-rich oxides (chromite and Cr-magnetite) were oversaturated in the water samples. Therefore, silicate minerals are the principal geogenic contributors of Cr and other major/minor elements (e.g., Mg^{2+}, Ca^{2+}, HCO_3^-, Si) and PTEs (e.g., As, Ni) to the spring waters of western Vermio Mt.

Table 6. The percentage distribution of the saturation state with respect to the selected mineral phases in the collected water samples.

Mineral Phase	Oversaturated SI > 0 (%)	Undersaturated SI < 0 (%)
Calcite	63.8	36.2
Dolomite	58.0	42.0
Magnesite	29.0	71.0
Talc	49.3	50.7
Chlorite	30.4	69.6
Tremolite	14.5	85.5
Enstatite	0.00	100
Diopside	0.00	100
Pyrolusite	0.00	100
Chromite	100	0.00
Magnetite	100	0.00
Chrysotile	14.5	85.5
Lizardite	14.5	85.5
Olivine (Forsterite)	0.00	100

4.3. NBLs of Cr in the Ultramafic Environment of Vermio Mt.

The geochemical characteristics of the natural springs, the geological environment, and the water–ultramafic rock interaction are reflected in springs' water quality. Chromium constitutes the principal environmental component in groundwater of the Sarigkiol Basin, originating primarily from geogenic and incidentally from anthropogenic sources [45]. This paper aims to assess the NBLs of Cr, which is of great interest in the catchment scale of the Sarigkiol Basin.

Based on the above-discussed hydrogeochemical data (e.g., pH, DO, Eh, Mg^{2+}, Si, Cr, alkalinity, etc.), the most representative natural springs, which flow through and interact with ultramafic rocks, are the S1-Agios Dimitrios area, "Mouratidis"-S2, "Potistis"-W13, and "Elafakia"-W14.

Take into consideration the modified methodology for assessing NBLs, the PS method was applied to create the new dataset. All samples from the natural springs satisfied the two criteria (ORP > 100 mV, DO > 3 mg/L and NO_3^- < 10 mg/L). Regarding the third criterion, the available time series of measurements, two natural springs, those of "Potistis"-W13 and "Elafakia"-W14, sufficiently satisfied this criterion. The resulting population was examined for the normality of the dataset with the Shapiro–Wilks test, a method proposed to be appropriate for a sample size less than 50 [80]. Although the number of the sampling sites is limited (2), they are considered representative because of the available time-series measurements, their hydrogeochemical characteristics, and the elevated concentrations of Cr, Si, Ni, and Mg^{2+}.

The normality test of Shapiro–Wilks showed that there was no normally distributed population of the samples, either for Cr or Cr(VI) ($p < 0.05$). The outliers were identified via Box plots to exclude these measurements in the next step until the total elimination of the outliers, and then the population of the remaining data was rechecked for its normal distribution (Figures 20 and 21). The last datasets of each parameter without outliers were double-checked for their normality with Q–Q plots and the Shapiro–Wilks test. In the spring "Elafakia"-W14, the NBLs of Cr constitutes the 95th percentile (57.24 μg/L) of the population as it was not normally distributed (Figure 20) [9]. On the other hand, Cr(VI) dataset was normally distributed, and based on the methodology, the NBL was defined to be 51.20 μg/L (NBL = the maximum value of the normally distributed dataset). Similarly, in the spring "Potistis"-W13, the NBLs of Cr is equal to the max value (130 μg/L) of the normally distributed dataset while the NBL for Cr(VI) was calculated at 100 μg/L (NBL = the 95th percentile of the dataset as non-normally distributed) (Figure 21).

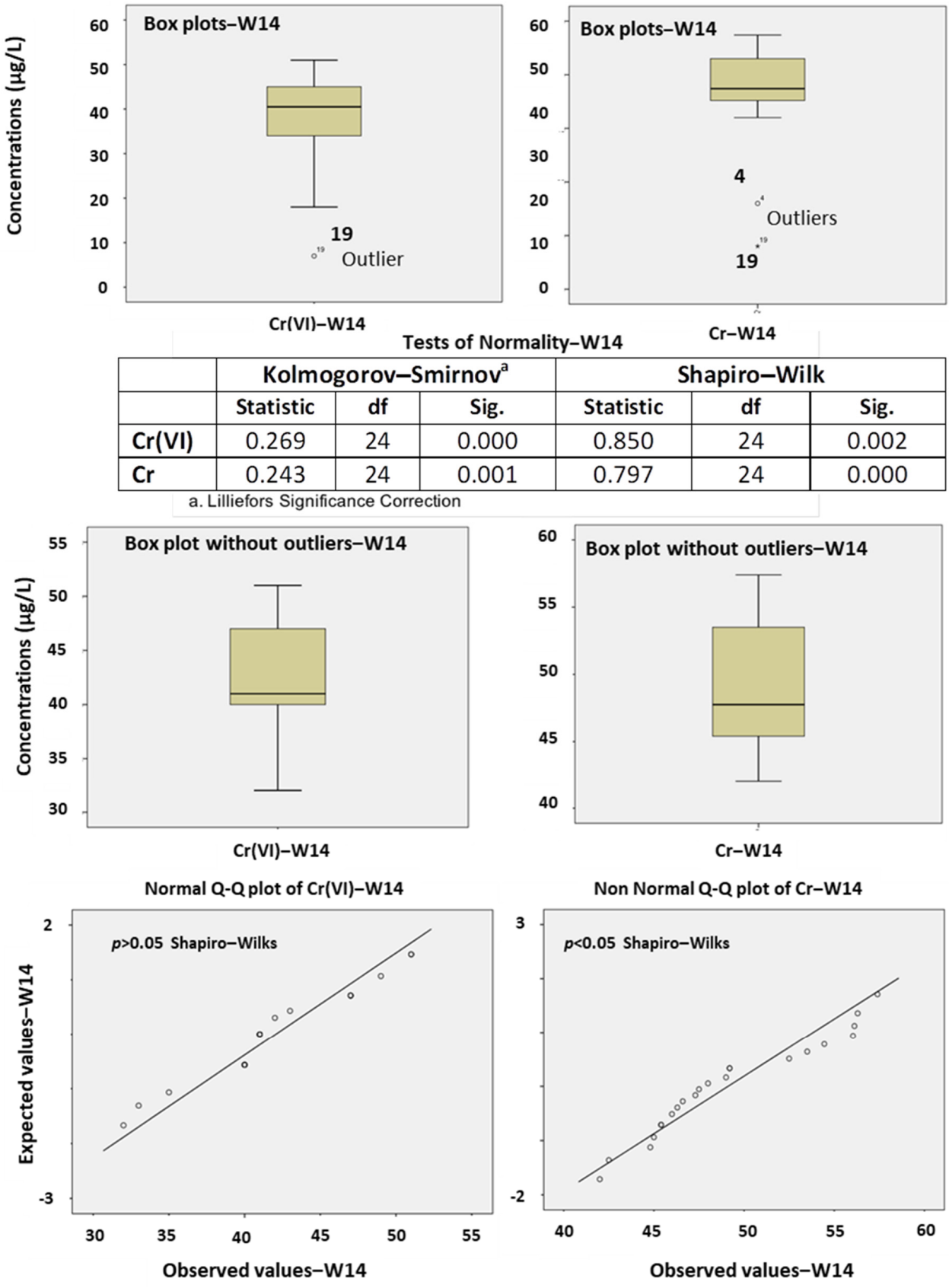

Tests of Normality–W14

	Kolmogorov–Smirnov[a]			Shapiro–Wilk		
	Statistic	df	Sig.	Statistic	df	Sig.
Cr(VI)	0.269	24	0.000	0.850	24	0.002
Cr	0.243	24	0.001	0.797	24	0.000

a. Lilliefors Significance Correction

Figure 20. Box plots and normality tests for the natural spring "Elafakia"-W14 in western Vermio Mt.

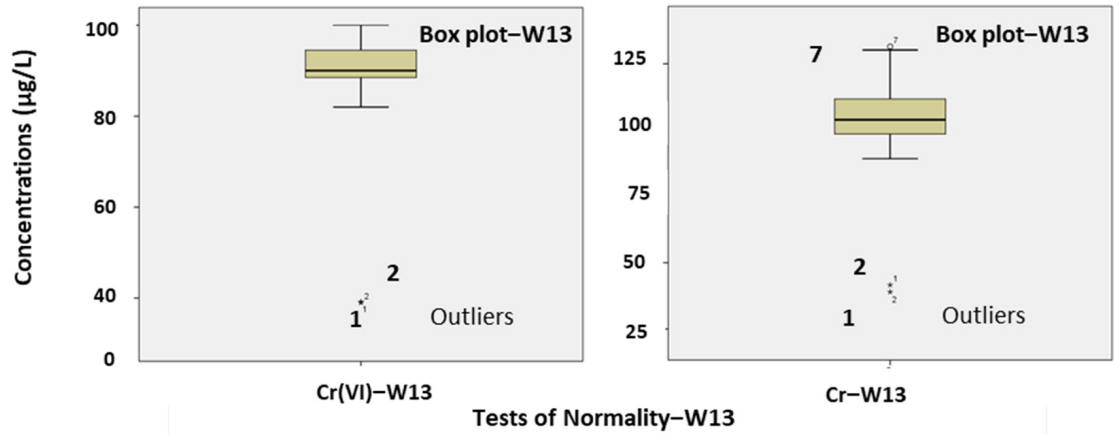

Tests of Normality–W13

	Kolmogorov–Smirnov[a]			Shapiro–Wilk		
	Statistic	df	Sig.	Statistic	df	Sig.
Cr(VI)	0.359	23	0.000	0.598	23	0.000
Cr	0.209	23	0.010	0.798	23	0.000

a. Lilliefors Significance Correction

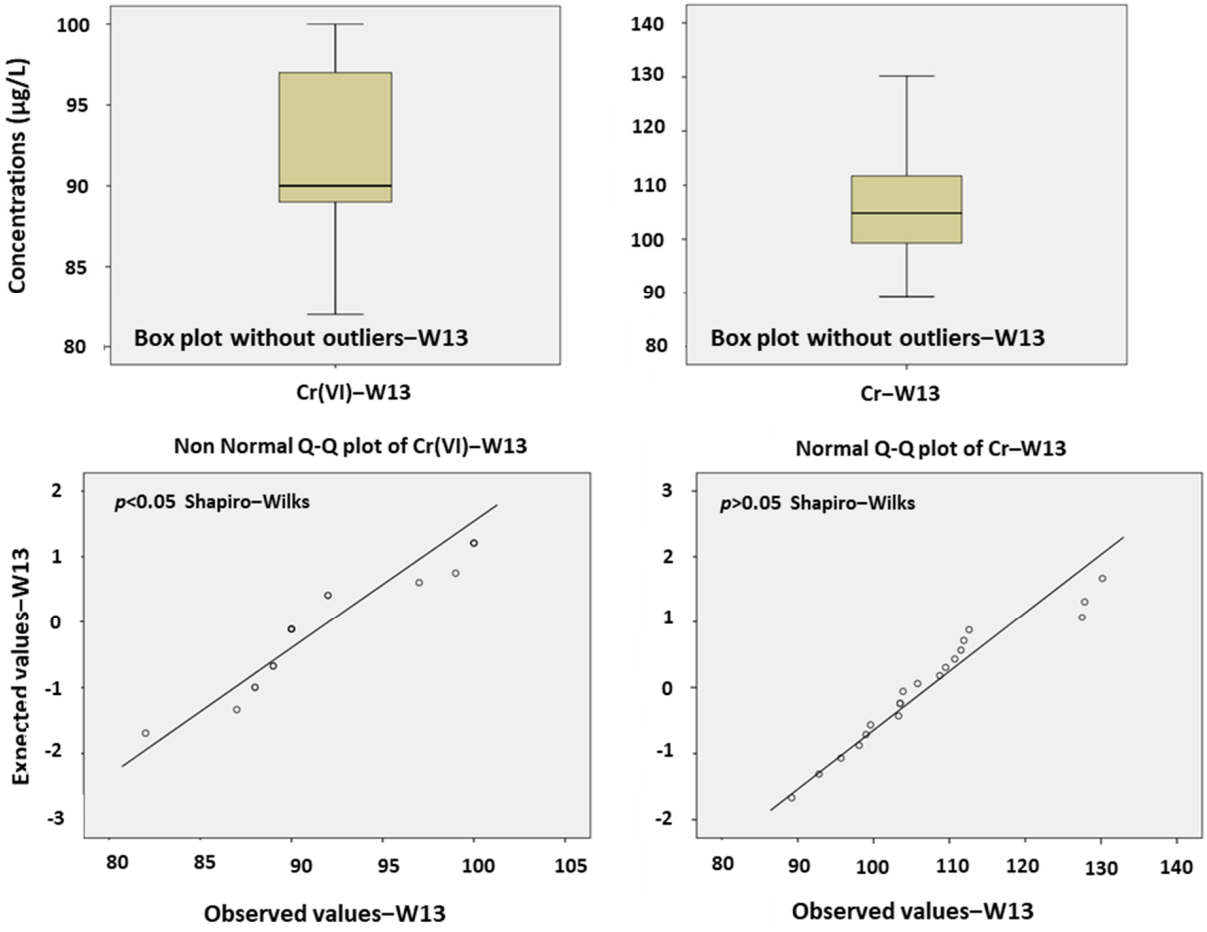

Figure 21. Box plots and normality tests for the natural spring "Potistis"-W13 in western Vermio Mt.

The estimated NBL is higher than the REF value (NBL/REF > 1) for both natural springs of Vermio. According to this suggestion, the TVs are determined as NBL for Cr in the natural springs of "Elafakia"-W14 and "Potistis"-W13. The spring "Potistis"-W13 is considered to be the most suitable one to define the NBLs in the ultramafic environment of

western Vermio Mt., because its water type (Mg-Ca-HCO_3) indicated a strong influence by ultramafic rocks, whereas the spring "Elafakia"-W14, with a Ca-Mg-HCO_3 water type, was mainly influenced by carbonate formations. In Figure 22, the flow chart describes the NBLs and TVs assessment for Cr and Cr(VI), for the natural spring "Potistis"-W13.

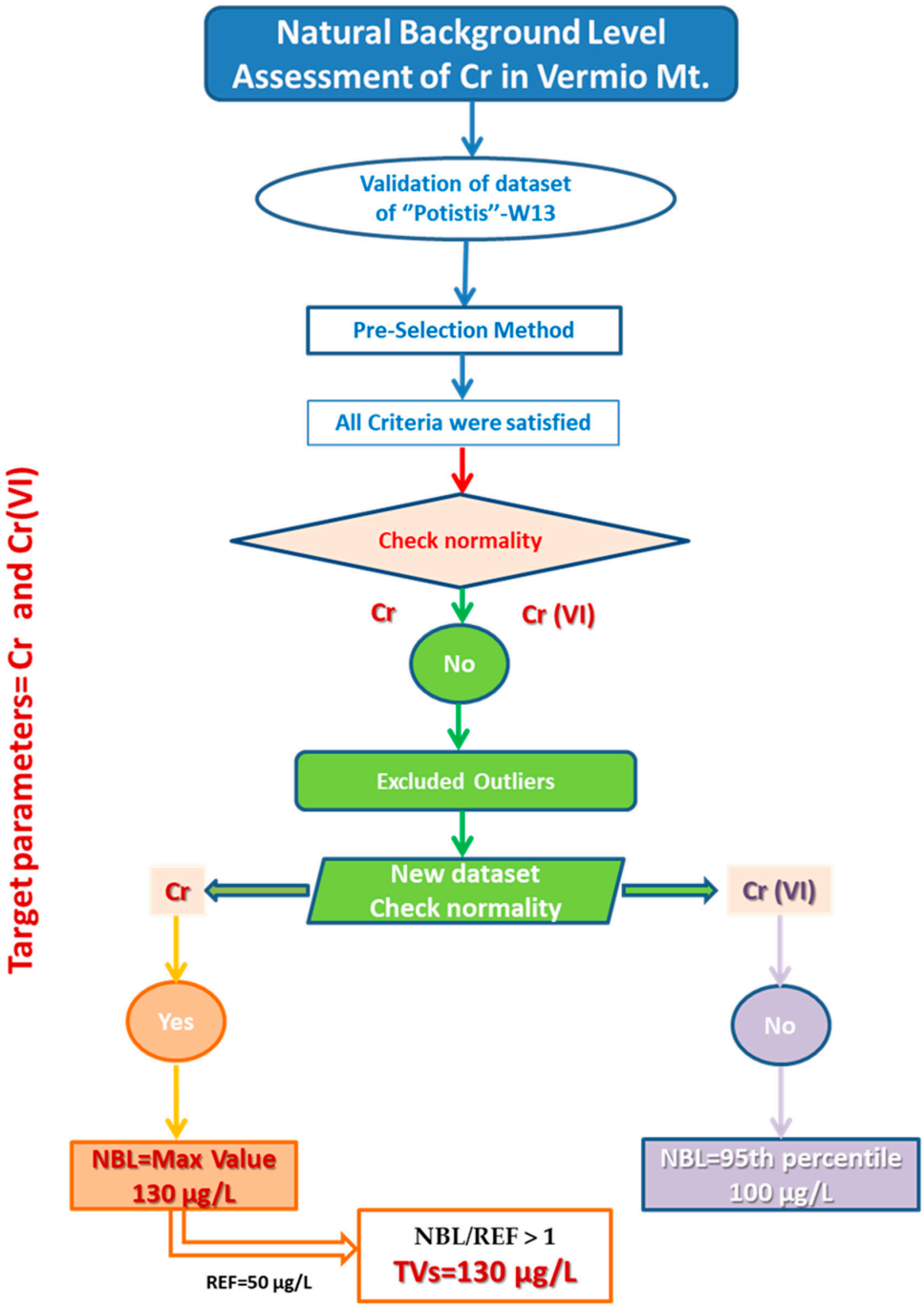

Figure 22. Flow chart of the modified conceptual model for assessing NBLs and TVs of Cr and Cr(VI) of the natural spring "Potistis"-W13, in western Vermio Mt.

The assessment of NBLs in ultramafic springs is a challenging modern methodology based on the continuous monitoring of hydrochemical parameters. Nevertheless, it is essential to mention that, since the environmental systems are complex and multicomponent, NBLs should not be treated as the absolute value above which a parameter is of anthropogenic origin; instead, NBLs constitute the minimum target value and the guide

for investigating elevated groundwater concentrations of a hydrogeochemical parameter and elucidating the influence of anthropogenic factors in a study area on a larger scale (e.g., at a catchment scale). The continued monitoring of water quality parameters is likely to provide higher concentrations of the specific parameters in the future, and therefore subsequent recalculation of NBLs may lead to higher NBLs in the study area.

The high potential leaching of Cr in Vermio Mt., as derived from the above-mentioned calculated NBLs, is imprinted in the lowland of the Sarigkiol Basin [45]. The surface runoff and the discharge of springs enriched in Cr follow various flow paths via torrents or streams through the weathered mantle of ultramafic rocks in western Vermio Mt. and leach into the lowland of the Sarigkiol Basin (Figure 23). Due to the hydraulic connection between the western Vermio Mt. and the eastern part of the lowland of the Sarigkiol Basin, the defined NBLs apply to the latter, supporting the dominance of the geogenic factor in the high groundwater concentration of Cr in the Sarigkiol Basin.

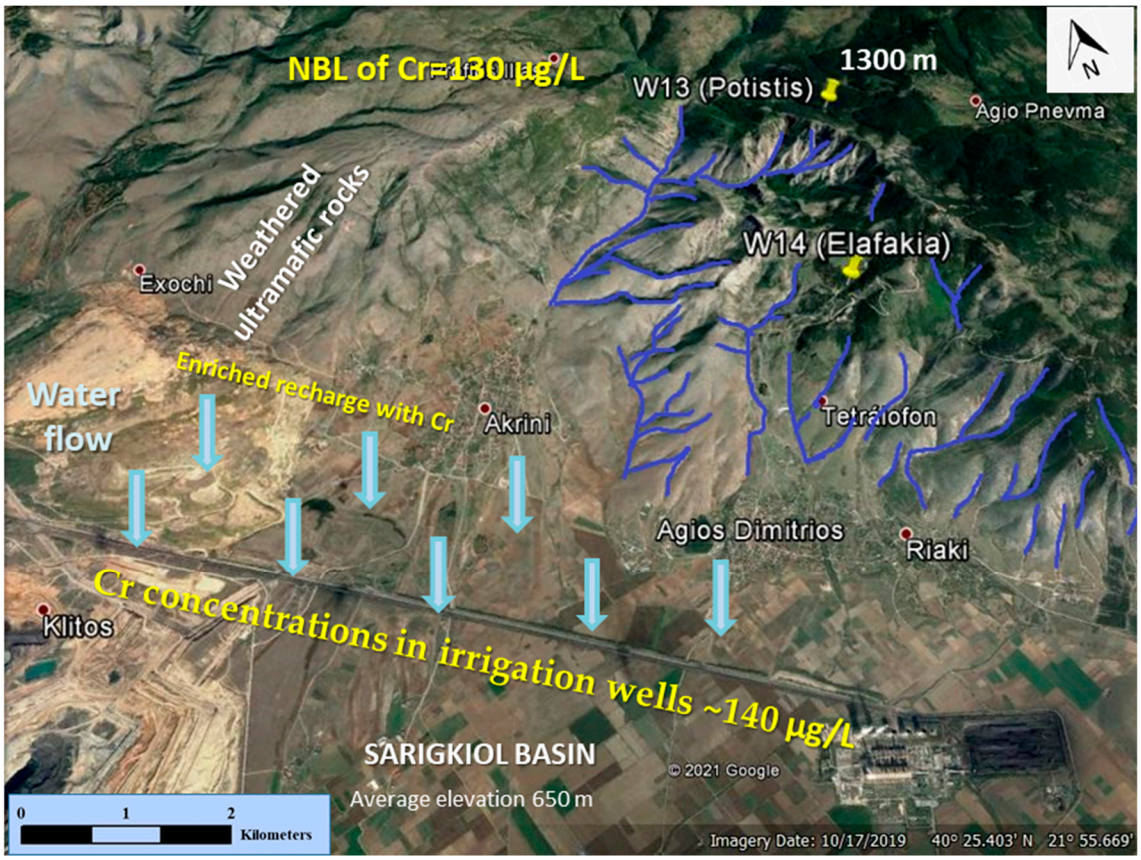

Figure 23. The flow paths and the natural recharge from western Vermio Mt. towards the eastern part of the Sarigkiol Basin (Google Earth image, 2021).

5. Conclusions

The ultramafic-dominated environment of western Vermio Mt. was fingerprinted on the groundwater chemistry and specifically on the elevated concentrations of Mg^{2+}, Si, Ni, and Cr in natural spring waters. Chromium was recognized as the principal environmental parameter in the natural spring waters of western Vermio Mt; in 42% of the studied spring water samples, the concentrations of Cr exceeded the WHO guideline value of 50 μg/L for drinking water. The geogenic origin of Cr in groundwater is recorded in the very strong positive correlation coefficients of Cr with Si, the strong positive correlation coefficients with Mg^{2+}, EC, and Ni, and the moderate positive correlation coefficients with HCO_3 and alkalinity.

The main factors that determined the concentration of Cr in the studied spring waters were:

(a) the time response of the aquifers systems to precipitations; direct infiltration on the geological formation of the aquifer results in immediate recharge of it. As a consequence, quick contaminant dilution takes place and fluctuations in Cr concentrations are observed depending on the time response of the aquifers to precipitation,
(b) the water–rock contact time; the longer the water–rock contact time is, the higher the Cr leaching is,
(c) the flow path of groundwater; a flow path through weathered ultramafic rocks results in the enrichment of groundwater in Cr,
(d) the degree of the serpentinisation of ultramafic rocks; the more serpentinised the ultramafic rocks are, the higher their leaching potential in Cr is, and
(e) the prevailing geochemical processes that favor the oxidation of Cr(III) to the soluble and mobile Cr(VI), such as alkaline pH, oxidative environment, presence of manganese oxides.

The absence of anthropic/anthropogenic activities in western Vermio Mt., the sufficient time-series data, and the hydrochemical characteristics of the studied springs allowed the assessment of NBLs of Cr by applying a multi-method approach. Considering the hydrogeological, hydrochemical, and hydrological data in western Vermio Mt. and applying the PS method, the spring "Potistis"-W13 was selected as the most representative one to define the NBLs of Cr in the area. The applied methodology is fully harmonized with the GDD and the Water Framework Directive (WFD, 2000/60/EC) [81]. The NBL of Cr was defined at 130 μg/L, and that of Cr(VI) at 100 μg/L. Based on the NBLs of Cr, TVs for Cr at a catchment scale, i.e., the Sarigkiol Basin, were defined to be equal to the NBLs. Conclusively, the ultramafic environment in western Vermio Mt. presents a high geochemical potential to dissolve and mobilize geogenic Cr.

This first systematic study of the natural springs of western Vermio Mt. provides important hydrogeochemical data for the geogenic footprint of a natural ultramafic environment on the groundwater quality. The proposed methodology could be implemented in any catchment scale aiming to distinguish between geogenic and anthropogenic groundwater deterioration and to establish new TVs considering the NBLs.

Author Contributions: Conceptualization, E.V. and M.P.; Data curation, E.V., M.P. and P.P.; Formal analysis, E.V., P.P. and M.P.; Investigation, E.V., P.P., M.P. and D.D.; Methodology, E.V., P.P. and M.P.; Project administration, M.P.; Supervision, M.P.; Visualization, E.V., P.P. and M.P.; Writing—original draft, E.V.; Writing—review and editing, E.V., P.P., M.P. and D.D. All authors have read and agreed to the summited version of the manuscript.

Funding: This research was carried out within the framework of the Research Project NTUA 623748.

Institutional Review Board Statement: Not applicable.

Informed Consent Statement: Not applicable.

Data Availability Statement: Some data is contained within the article. All hydrogeochemical data may be available for collaborative research projects by specific agreements. For information, contact maria@metal.ntua.gr.

Acknowledgments: Special thanks to G. Stamatis, Emeritus Professor in Hydrogeology (Agricultural University of Athens) and A. Dimitriadis, from Agios Dimitrios Power Plant of Public Power Corporation for their contribution to the fieldwork. A. Stamos in EAGME is acknowledged for valuable discussion on the operation mechanisms of the springs in western Vermio Mt. We would like to thank the two anonymous reviewers for their constructive com-ments and suggestions that significantly improved the quality of the paper. Special thanks are ex-pressed to the editors for their careful editorial handling.

Conflicts of Interest: The authors declare no conflict of interest.

References

1. European Union. EU Groundwater Directive 2006/118/EC. *Off. J. Eur. Union* **2006**, *L 372*, 19–31.
2. Amiri, V.; Nakhaei, M.; Lak, R.; Li, P. An integrated statistical-graphical approach for the appraisal of the natural background levels of some major ions and potentially toxic elements in the groundwater of Urmia aquifer, Iran. *Environ. Earth Sci.* **2021**, *80*, 432. [CrossRef]
3. Edmunds, W.; Shand, P.; Hart, P.; Ward, R. The natural (baseline) quality of groundwater: A UK pilot study. *Sci. Total. Environ.* **2003**, *310*, 25–35. [CrossRef]
4. Gemitzi, A. Evaluating the anthropogenic impacts on groundwaters: A methodology based on the determination of natural background levels and threshold values. *Environ. Earth Sci.* **2012**, *67*, 2223–2237. [CrossRef]
5. Preziosi, E.; Giuliano, G.; Vivona, R. Natural background levels and threshold values derivation for naturally As, V and F rich groundwater bodies: A methodological case study in Central Italy. *Environ. Earth Sci.* **2009**, *61*, 885–897. [CrossRef]
6. Urresti-Estala, B.; Carrasco-Cantos, F.; Pérez, I.V.; Gavilán, P.J. Determination of background levels on water quality of groundwater bodies: A methodological proposal applied to a Mediterranean River basin (Guadalhorce River, Málaga, Southern Spain). *J. Environ. Manag.* **2013**, *117*, 121–130. [CrossRef] [PubMed]
7. Sacchi, E.; Bergamini, M.; Lazzari, E.; Musacchio, A.; Mor, J.-R.; Pugliaro, E. Natural Background Levels of Potentially Toxic Elements in Groundwater from a Former Asbestos Mine in Serpentinite (Balangero, North Italy). *Water* **2021**, *13*, 735. [CrossRef]
8. Libera, N.D.; Fabbri, P.; Mason, L.; Piccinini, L.; Pola, M. A local natural background level concept to improve the natural background level: A case study on the drainage basin of the Venetian Lagoon in Northeastern Italy. *Environ. Earth Sci.* **2018**, *77*, 487. [CrossRef]
9. Parrone, D.; Ghergo, S.; Preziosi, E. A multi-method approach for the assessment of natural background levels in groundwater. *Sci. Total. Environ.* **2018**, *659*, 884–894. [CrossRef] [PubMed]
10. Preziosi, E.; Parrone, D.; del Bon, A.; Ghergo, S. Natural background level assessment in groundwaters: Probability plot versus pre-selection method. *J. Geochem. Explor.* **2014**, *143*, 43–53. [CrossRef]
11. Muller, D.; Blum, A.; Hart, A.; Hookey, J.; Kunkel, R.; Scheidleder, A.; Tomlin, C.; Wendland, F. *D18: Final Proposal for a Methodology to Set Up Groundwater Threshold Values in Europe*; Background Criteria for the Identification of Groundwater Thresholds; Bridge Publications: Vienna, Austria, 2006.
12. Wendland, F.; Berthold, G.; Blum, A.; Elsass, P.; Fritsche, J.-G.; Kunkel, R.; Wolter, R. Derivation of natural background levels and threshold values for groundwater bodies in the Upper Rhine Valley (France, Switzerland and Germany). *Desalination* **2008**, *226*, 160–168. [CrossRef]
13. Hinsby, K.; de Melo, M.T.C.; Dahl, M. European case studies supporting the derivation of natural background levels and groundwater threshold values for the protection of dependent ecosystems and human health. *Sci. Total Environ.* **2008**, *401*, 1–20. [CrossRef]
14. Ducci, D.; de Melo, M.T.C.; Preziosi, E.; Sellerino, M.; Parrone, D.; Ribeiro, L. Combining natural background levels (NBLs) assessment with indicator kriging analysis to improve groundwater quality data interpretation and management. *Sci. Total Environ.* **2016**, *569–570*, 569–584. [CrossRef] [PubMed]
15. Biddau, R.; Cidu, R.; Lorrai, M.; Mulas, M. Assessing background values of chloride, sulfate and fluoride in groundwater: A geochemical-statistical approach at a regional scale. *J. Geochem. Explor.* **2017**, *181*, 243–255. [CrossRef]
16. Masciale, R.; Amalfitano, S.; Frollini, E.; Ghergo, S.; Melita, M.; Parrone, D.; Preziosi, E.; Vurro, M.; Zoppini, A.; Passarella, G. Assessing Natural Background Levels in the Groundwater Bodies of the Apulia Region (Southern Italy). *Water* **2021**, *13*, 958. [CrossRef]
17. Filippini, M.; Zanotti, C.; Bonomi, T.; Sacchetti, V.; Amorosi, A.; Dinelli, E.; Rotiroti, M. Deriving Natural Background Levels of Arsenic at the Meso-Scale Using Site-Specific Datasets: An Unorthodox Method. *Water* **2021**, *13*, 452. [CrossRef]
18. Oze, C.; Fendorf, S.; Bird, D.K.; Coleman, R.G. Chromium geochemistry in serpentinized ultramafic rocks and serpentine soils from the Franciscan complex of California. *Am. J. Sci.* **2004**, *304*, 67–101. [CrossRef]
19. Tashakor, M.; Modabberi, S.; van der Ent, A.; Echevarria, G. Impacts of ultramafic outcrops in Peninsular Malaysia and Sabah on soil and water quality. *Environ. Monit. Assess.* **2018**, *190*, 333. [CrossRef] [PubMed]
20. Kelepertzis, E.; Galanos, E.; Mitsis, I. Origin, mineral speciation and geochemical baseline mapping of Ni and Cr in agricultural topsoils of Thiva Valley (central Greece). *J. Geochem. Explor.* **2013**, *125*, 56–68. [CrossRef]
21. Ryan, P.C.; Kim, J.; Wall, A.J.; Moen, J.C.; Corenthal, L.G.; Chow, D.R.; Sullivan, C.M.; Bright, K.S. Ultramafic-derived arsenic in a fractured bedrock aquifer. *Appl. Geochem.* **2011**, *26*, 444–457. [CrossRef]
22. Nriagu, J.; Nieboer, E. *Chromium in the Natural and Human Environments*; John Wiley & Sons: New York, NY, USA, 1988; Volume 20.
23. Rai, D.; Sass, B.M.; Moore, D.A. Chromium(III) hydrolysis constants and solubility of chromium(III) hydroxide. *Inorg. Chem.* **1987**, *26*, 345–349. [CrossRef]
24. Sperling, M.; Xu, S.; Welz, B. Determination of chromium(III) and chromium(VI) in water using flow injection on-line preconcentration with selective adsorption on activated alumina and flame atomic absorption spectrometric detection. *Anal. Chem.* **1992**, *64*, 3101–3108. [CrossRef]
25. Kotaś, J.; Stasicka, Z. Chromium occurrence in the environment and methods of its speciation. *Environ. Pollut.* **2000**, *107*, 263–283. [CrossRef]

26. Berna, E.C.; Johnson, T.M.; Makdisi, R.S.; Basu, A. Cr Stable Isotopes As Indicators of Cr(VI) Reduction in Groundwater: A Detailed Time-Series Study of a Point-Source Plume. *Environ. Sci. Technol.* **2009**, *44*, 1043–1048. [CrossRef] [PubMed]
27. Johnson, C.; Xyla, A.G. The oxidation of chromium(III) to chromium(VI) on the surface of manganite (γ-MnOOH). *Geochim. Cosmochim. Acta* **1991**, *55*, 2861–2866. [CrossRef]
28. Fendorf, S.E.; Fendorf, M.; Sparks, D.L.; Gronsky, R. Inhibitory mechanisms of Cr(III) oxidation by δ-MnO2. *J. Colloid Interface Sci.* **1992**, *153*, 37–54. [CrossRef]
29. Fantoni, D.; Brozzo, G.; Canepa, M.; Cipolli, F.; Marini, L.; Ottonello, G.; Zuccolini, M. Natural hexavalent chromium in groundwaters interacting with ophiolitic rocks. *Environ. Earth Sci.* **2002**, *42*, 871–882. [CrossRef]
30. Tziritis, E.; Kelepertzis, E.; Korres, G.; Perivolaris, D.; Repani, S. Hexavalent Chromium Contamination in Groundwaters of Thiva Basin, Central Greece. *Bull. Environ. Contam. Toxicol.* **2012**, *89*, 1073–1077. [CrossRef] [PubMed]
31. Dermatas, D.; Mpouras, T.; Chrysochoou, M.; Panagiotakis, I.; Vatseris, C.; Linardos, N.; Theologou, E.; Boboti, N.; Xenidis, A.; Papassiopi, N.; et al. Origin and concentration profile of chromium in a Greek aquifer. *J. Hazard. Mater.* **2015**, *281*, 35–46. [CrossRef] [PubMed]
32. Hausladen, D.M.; Alexander-Ozinskas, A.; McClain, C.N.; Fendorf, S. Hexavalent Chromium Sources and Distribution in California Groundwater. *Environ. Sci. Technol.* **2018**, *52*, 8242–8251. [CrossRef]
33. Papazotos, P.; Vasileiou, E.; Perraki, M. Elevated groundwater concentrations of arsenic and chromium in ultramafic environments controlled by seawater intrusion, the nitrogen cycle, and anthropogenic activities: The case of the Gerania Mountains, NE Peloponnese, Greece. *Appl. Geochem.* **2020**, *121*, 104697. [CrossRef]
34. Coyte, R.; McKinley, K.; Jiang, S.; Karr, J.; Dwyer, G.S.; Keyworth, A.J.; Davis, C.C.; Kondash, A.J.; Vengosh, A. Occurrence and distribution of hexavalent chromium in groundwater from North Carolina, USA. *Sci. Total. Environ.* **2019**, *711*, 135135. [CrossRef]
35. Perraki, M.; Vasileiou, E.; Bartzas, G. Tracing the origin of chromium in groundwater: Current and new perspectives. *Curr. Opin. Environ. Sci. Heal.* **2021**, *22*, 100267. [CrossRef]
36. Vithanage, M.; Kumarathilaka, P.; Oze, C.; Karunatilake, S.; Seneviratne, M.; Hseu, Z.-Y.; Gunarathne, V.; Dassanayake, M.; Ok, Y.S.; Rinklebe, J. Occurrence and cycling of trace elements in ultramafic soils and their impacts on human health: A critical review. *Environ. Int.* **2019**, *131*, 104974. [CrossRef]
37. Liang, J.; Huang, X.; Yan, J.; Li, Y.; Zhao, Z.; Liu, Y.; Ye, J.; Wei, Y. A review of the formation of Cr(VI) via Cr(III) oxidation in soils and groundwater. *Sci. Total Environ.* **2021**, *774*, 145762. [CrossRef]
38. Papazotos, P.; Vasileiou, E.; Perraki, M. The synergistic role of agricultural activities in groundwater quality in ultramafic environments: The case of the Psachna basin, central Euboea, Greece. *Environ. Monit. Assess.* **2019**, *191*, 317. [CrossRef]
39. Oze, C.; Bird, D.K.; Fendorf, S. Genesis of hexavalent chromium from natural sources in soil and groundwater. *Proc. Natl. Acad. Sci. USA* **2007**, *104*, 6544–6549. [CrossRef] [PubMed]
40. Margiotta, S.; Mongelli, G.; Summa, V.; Paternoster, M.; Fiore, S. Trace element distribution and Cr(VI) speciation in Ca-HCO_3 and Mg-HCO_3 spring waters from the northern sector of the Pollino massif, Southern Italy. *J. Geochem. Explor.* **2012**, *115*, 1–12. [CrossRef]
41. Remoundaki, E.; Vasileiou, E.; Philippou, A.; Perraki, M.; Kousi, P.; Hatzikioseyian, A.; Stamatis, G. Groundwater Deteriora-tion: The Simultaneous Effects of Intense Agricultural Activity and Heavy Metals in Soil. *Procedia Eng.* **2016**, *162*, 545–552. [CrossRef]
42. Kaprara, E.; Kazakis, N.; Simeonidis, K.; Coles, S.; Zouboulis, A.; Samaras, P.; Mitrakas, M. Occurrence of Cr(VI) in drinking water of Greece and relation to the geological background. *J. Hazard. Mater.* **2014**, *281*, 2–11. [CrossRef]
43. Elango, L.; Kannan, R. *Chapter 11: Rock–Water Interaction and Its Control on Chemical Composition of Groundwater*; Elsevier: Amsterdam, The Netherlands, 2007; pp. 229–243. [CrossRef]
44. Sharif, M.; Davis, R.; Steele, K.; Kim, B.; Kresse, T.; Fazio, J. Inverse geochemical modeling of groundwater evolution with emphasis on arsenic in the Mississippi River Valley alluvial aquifer, Arkansas (USA). *J. Hydrol.* **2008**, *350*, 41–55. [CrossRef]
45. Vasileiou, E.; Papazotos, P.; Dimitrakopoulos, D.; Perraki, M. Expounding the origin of chromium in groundwater of the Sarigkiol Basin, Western Macedonia, Greece: A cohesive statistical approach and hydrochemical study. *Environ. Monit. Assess.* **2019**, *191*, 509. [CrossRef] [PubMed]
46. Stamos, A.; Samiotis, G.; Tsioptsias, C.; Amanatidou, E. Natural presence of hexavalent chromium in spring waters of South-West Mountain Vermion, Greece. In Proceedings of the 16th International Conference on Environmental Science and Technology (CEST 2019), Rhodes, Greece, 4–7 September 2019; p. 4.
47. Institute of Geology and Mineral Exploration of Greece. *Geological Maps of Greece, Sheet: Kozani*; Scale 1:50.000, Department of Geological Maps; Institute of Geology and Mineral Exploration of Greece: Athens, Greece, 1980.
48. Perraki, M. *Mineralogical, Petrological and Geochemical Study of Heavy Minerals with Emphasis on Chromium in the Geological Formations (Ultrabasic Rocks, Lignite, Clay Formations) and the Coal-Fired Products (Fly Ash) and the Quality of Surficial and Underground Aquifers of the Sarigkiol Basin (NW Greece)*; Technical Report; National Technical University of Athesn: Athens, Greece, 2016.
49. Nematollahi, M.J.; Ebrahimi, P.; Razmara, M.; Ghasemi, A. Hydrogeochemical investigations and groundwater quality assessment of Torbat-Zaveh plain, Khorasan Razavi, Iran. *Environ. Monit. Assess.* **2015**, *188*, 1–21. [CrossRef]
50. Esmaeili, A.; Moore, F. Hydrogeochemical assessment of groundwater in Isfahan province, Iran. *Environ. Earth Sci.* **2011**, *67*, 107–120. [CrossRef]
51. Spearman, C. The Proof and Measurement of Association between Two Things. *Am. J. Psychol.* **1904**, *15*, 72. [CrossRef]
52. Wuensch, K.L.; Evans, J.D. Straightforward Statistics for the Behavioral Sciences. *J. Am. Stat. Assoc.* **1996**, *91*, 1750. [CrossRef]

53. Gauthier, T. Detecting Trends Using Spearman's Rank Correlation Coefficient. *Environ. Forensics* **2001**, *2*, 359–362. [CrossRef]
54. Wilk, M.B.; Gnanadesikan, R. Probability plotting methods for the analysis for the analysis of data. *Biometrika* **1968**, *55*, 1–17. [CrossRef]
55. Parkhurst, D.L.; Appelo, C.A.J. *User's Guide to PHREEQC (Version 2): A Computer Program for Speciation, Batch-Reaction, One-Dimensional Transport, and Inverse Geochemical Calculations*; U.S. Geological Survey, Water Resources Investigations Report 99-4259; United States Geological Survey (USGS): Washington, DC, USA, 1999.
56. Merkel, B.J.; Planer-Friedrich, B.; Nordstrom, D.K. *Groundwater Geochemistry: A Practical Guide to Modeling of Natural and Contaminated Aquatic Systems*; Springer: Berlin, Germany, 2005.
57. Zhang, F.; Jin, Z.; Yu, J.; Zhou, Y.; Zhou, L. Hydrogeochemical processes between surface and groundwaters on the north-eastern Chinese Loess Plateau: Implications for water chemistry and environmental evolutions in semi-arid regions. *J. Geochem. Explor.* **2015**, *159*, 115–128. [CrossRef]
58. Christoforidou, P.; Panagopoulos, A.; Voudouris, K. Towards A New Procedure To Set Up Groundwater Threshold Values In Accordance With The Previsions Of The Ec Directive 2006/118: A Case Study From Achaia And Corinthia (Greece). *Bull. Geol. Soc. Greece* **2017**, *43*, 1678. [CrossRef]
59. Molinari, A.; Guadagnini, L.; Marcaccio, M.; Guadagnini, A. Natural background levels and threshold values of chemical species in three large-scale groundwater bodies in Northern Italy. *Sci. Total Environ.* **2012**, *425*, 9–19. [CrossRef] [PubMed]
60. Chidichimo, F.; de Biase, M.; Straface, S. Groundwater pollution assessment in landfill areas: Is it only about the leachate? *Waste Manag.* **2019**, *102*, 655–666. [CrossRef] [PubMed]
61. Parrone, D.; Frollini, E.; Preziosi, E.; Ghergo, S. eNaBLe, an On-Line Tool to Evaluate Natural Background Levels in Groundwater Bodies. *Water* **2020**, *13*, 74. [CrossRef]
62. Masetti, M.; Poli, S.; Sterlacchini, S.; Beretta, G.P.; Facchi, A. Spatial and statistical assessment of factors influencing nitrate contamination in groundwater. *J. Environ. Manag.* **2008**, *86*, 272–281. [CrossRef] [PubMed]
63. Menció, A.; Mas-Pla, J.; Otero, N.; Regàs, O.; Boy-Roura, M.; Puig, R.; Bach, J.; Domènech, C.; Zamorano, M.; Brusi, D.; et al. Nitrate pollution of groundwater; all right, but nothing else? *Sci. Total Environ.* **2016**, *539*, 241–251. [CrossRef] [PubMed]
64. Soltan, M.E. Evaluation Of Ground Water Quality In Dakhla Oasis (Egyptian Western Desert). *Environ. Monit. Assess.* **1999**, *57*, 157–168. [CrossRef]
65. Singh, U.V.; Abhishek, A.; Singh, K.P.; Dhakate, R.; Singh, N.P. Groundwater quality appraisal and its hydrochemical characterization in Ghaziabad (a region of indo-gangetic plain), Uttar Pradesh, India. *Appl. Water Sci.* **2013**, *4*, 145–157. [CrossRef]
66. World Health Organization. *Guidelines for Drinking-Water Quality*, 4th ed.; World Health Organization: Geneva, Switzerland, 2011.
67. Marghade, D.; Malpe, D.B.; Zade, A.B. Geochemical characterization of groundwater from northeastern part of Nagpur urban, Central India. *Environ. Earth Sci.* **2010**, *62*, 1419–1430. [CrossRef]
68. Lelli, M.; Grassi, S.; Amadori, M.; Franceschini, F. Natural Cr(VI) contamination of groundwater in the Cecina coastal area and its inner sectors (Tuscany, Italy). *Environ. Earth Sci.* **2013**, *71*, 3907–3919. [CrossRef]
69. Barnes, I.; O'neil, J.R. The relationship between fluids in some fresh alpine-type ultramafics and possible modern ser-pentinization, Western United States. *Bull. Geol. Soc. Am.* **1969**, *80*, 1947–1960. [CrossRef]
70. Cipolli, F.; Gambardella, B.; Marini, L.; Ottonello, G.; Zuccolini, M.V. Geochemistry of high-pH waters from serpentinites of the Gruppo di Voltri (Genova, Italy) and reaction path modeling of CO_2 sequestration in serpentinite aquifers. *Appl. Geochem.* **2004**, *19*, 787–802. [CrossRef]
71. Marques, J.M.; Carreira, P.M.; Carvalho, M.D.R.; Matias, M.J.; Goff, F.E.; Basto, M.J.; Graça, R.C.; Aires-Barros, L.; Rocha, L. Origins of high pH mineral waters from ultramafic rocks, Central Portugal. *Appl. Geochem.* **2008**, *23*, 3278–3289. [CrossRef]
72. Richard, F.C.; Bourg, A.C. Aqueous geochemistry of chromium: A review. *Water Res.* **1991**, *25*, 807–816. [CrossRef]
73. Zhang, B.; Zhao, D.; Zhou, P.; Qu, S.; Liao, F.; Guangcai, W. Hydrochemical Characteristics of Groundwater and Dominant Water—Rock Interactions in the Delingha. *Water* **2020**, *12*, 836. [CrossRef]
74. Redwan, M.; Moneim, A.A.A.; Amra, M.A. Effect of water–rock interaction processes on the hydrogeochemistry of ground-water west of Sohag area, Egypt. *Arab. J. Geosci.* **2016**, *9*, 111. [CrossRef]
75. Jalali, M.; Khanlari, Z.V. Cadmium Availability in Calcareous Soils of Agricultural Lands in Hamadan, Western Iran. Soil Sediment. Contam. *Int. J.* **2008**, *17*, 256–268. [CrossRef]
76. Gibbs, R.J. Mechanisms Controlling World Water Chemistry. *Science* **1970**, *170*, 1088–1090. [CrossRef] [PubMed]
77. Marandi, A.; Shand, P. Groundwater chemistry and the Gibbs Diagram. *Appl. Geochem.* **2018**, *97*, 209–212. [CrossRef]
78. McClain, C.; Maher, K. Chromium fluxes and speciation in ultramafic catchments and global rivers. *Chem. Geol.* **2016**, *426*, 135–157. [CrossRef]
79. Giammetta, R.; Telesca, A.; Mongelli, G. Serpentinites-water interaction in the S. Severino area, Lucanian Apennines, Southern Italy. *GeoActa* **2004**, *3*, 25–33.
80. Hanusz, Z.; Tarasińska, J. Normalization of the Kolmogorov–Smirnov and Shapiro–Wilk tests of normality. *Biom. Lett.* **2015**, *52*, 85–93. [CrossRef]
81. EUROPA. European Commission Water Framework Directive 2000/60/EC. *Off. J. Eur. Communities* **2000**, *L 327*, 1–73.